Neutrophil extracellular traps exacerbate microglia/macrophages-mediated neuroinflammation via cGAS in mice with traumatic brain injury

mingming shi
Tianjin Medical University General Hospital
Liang Liu
Tianjin Medical University General Hospital
Yiyao Cao
Tianjin Medical University General Hospital
Xiaobin Min
Tianjin Medical University
tuo li
Haoran Jia
Tianjin Medical University General Hospital
Liang Mi
Tianjin Medical University General Hospital
Yanfeng Zhang
Tianjin Medical University General Hospital
Xilei Liu
Tianjin Medical University General Hospital
Yuan Zhou
Tianjin Medical University General Hospital
Shenghui Li
Tianjin Medical University General Hospital
Guili Yang
Tianjin Medical University General Hospital
Xiao Liu
Tianjin Medical University General Hospital
Quanjun Deng
Tianjin Medical University General Hospital
Fanglian Chen
Tianjin Medical University General Hospital
xin chen

Tianjin Medical University General Hosptial
Shu Zhang (zhangshu2017@tmu.edu.cn)
Tianjin Medical University General Hospital
Jianning Zhang
Tianjin Medical University General Hospital

Article

Keywords: Traumatic brain injury, Microglia/macrophage, Neutrophil extracellular trap, cGAS, STING

Posted Date: November 22nd, 2022

DOI: https://doi.org/10.21203/rs.3.rs-2252334/v1

Abstract

Intense neuroinflammatory response with widespread microglia/macrophage activation and leucocyte infiltration occurring during the acute phase of traumatic brain injury (TBI) is an important mediator of secondary neurological injury. Neutrophils, as the most abundant leukocytes in peripheral circulation and the first-line transmigrated immune cells at the contused parenchyma following TBI, are suggested to worsen TBI outcomes and exacerbate TBI-related neuroinflammation, via unclear mechanisms. We hypothesized that neutrophil extracellular trap (NET) formation as a key mechanistic regulator, exacerbate microglia/macrophage-mediated neuroinflammation and acute neurological deficits after TBI. In this study, we observed massive NET formation in contused brain tissue of TBI patients and elevated plasma NET biomarkers correlated with upregulated cGAS-STING pathway. Overexpression of peptidylarginine deiminase 4 (PAD4) induces an increase in the NET formation that is accompanied by upregulation of the cGAS-STING pathway and exacerbation of microglia/macrophages-mediated neuroinflammation and neurological injury. Additionally, degradation of NETs-associated DNA by DNase 1 and inhibition of NET formation by pharmacological inhibition of PAD effectively inhibit cGAS-STING pathway activation and ameliorate microglia/macrophages-mediated neuroinflammatory responses. Collectively, our data highlight that targeting NETs is a promising therapeutic strategy for TBI treatment.

Introduction

Traumatic brain injury (TBI) remains one of the leading causes of death and devastating diseases worldwide across all age groups [1]. Recent evidence suggests that a non-resolving neuroinflammatory response with widespread microglia/macrophage activation following TBI is critical secondary injury pathogenesis that can drive ongoing neuronal injury, resulting in motor and cognitive function deficits [2]. During the initial injury phase, functional microglia/macrophages recognize damage-associated molecular patterns and migrate toward injury sites, contributing to the clearance of cellular debris and orchestration of tissue repair [3]. However, numerous microglia/macrophages retain an active M1-like phenotype well into the secondary phase of TBI, with an amoeboid appearance. These active microglia/macrophages undergo pyroptosis, releasing a series of detrimental pro-inflammatory cytokines [4]. Therefore, targeting the inhibition of microglia/macrophage activation is of great therapeutic interest to improve recovery following TBI.

Neutrophils, the short-lived, peripheral innate immune cells recruited to the lesion parenchyma after TBI, present a key event during neuroinflammation post-injury [5]. Existing evidence has confirmed that depletion of neutrophils or elimination of neutrophil recruitment protects against brain injury [5]. Functionally, neutrophil depletion ameliorates microcirculatory dysfunction and edema after TBI [6]. Previous studies have demonstrated that activated microglia recruit and activate neutrophils by releasing a series of inflammatory cytokines and chemokines [7–9]. Reciprocally, activated neutrophils promote microglial activation by releasing reactive oxygen species (ROS), lipocalin, and matrix metalloproteinase-9 (MMP9) [5]. Furthermore, previous studies have shown that massive neutrophils infiltrate the brain parenchyma and directly interact with microglia using intravital intracranial two-photon microscopy in a

mouse model of stroke [10, 11]. However, it remains unclear whether neutrophil infiltration is present in the brain parenchyma of TBI patients and whether infiltrated neutrophils influence microglia/macrophages -mediated pro-inflammatory responses. Furthermore, the underlying mechanism is also unknown after TBI.

Various mechanisms of neutrophil-mediated immune responses have been proposed, including neutrophil extracellular traps (NETs), an extracellular web-like structure released by neutrophils, which have been recently identified as a novel mechanism contributing to exacerbation of inflammation [12], the onset of autoimmune disorders [13] and thrombi formation [14]. NETs are composed of extracellular double-stranded DNA combined with several components, including histones, neutrophil elastase, myeloperoxidase (MPO), and cathepsin [15]. NETs have been found in the brain parenchyma [16] and cerebrovascular thrombi [17] of ischemic stroke patients and inhibition of NETs formation could improve stroke outcomes [16]. Functionally, a recent study reported increased NET in the plasma of patients with severe TBI, which correlates with elevated ICP and worse neurological function [18]. However, whether NETs are present in the brain parenchyma of TBI patients and whether neutrophil-released NETs are a key mechanism by which infiltrated neutrophils are involved in microglial activation during TBI acute phase remains unclear. Thus, we obtained preoperative blood samples and postoperative brain tissue specimens from several TBI patients and analyzed the level of circulating NET formation in the blood samples and neutrophil-dependent NET formation in the brain tissue specimens. Subsequently, we sought to determine whether targeting neutrophils and NETs could ameliorate microglia/macrophage-mediated neuroinflammation, improve neurological deficits, and uncover the mechanisms of M1 polarization and pyroptosis of microglia/macrophages triggered by NETs in a mouse model of TBI.

Materials And Methods

Human brain tissues

Human brain tissues were obtained in accordance with an ethically reviewed and approved protocol from Tianjin Medical University General Hospital. Six patients with severe TBI, defined as post-resuscitation Glasgow coma scale (GCS) scores less than 8, were included. Control brain specimens were obtained from four patients with glioma who underwent maximizing resection of malignant glioma to improve survival. None of the patients had any other known neurological disorder. The demographics and clinical characteristics of these patients are shown in Table 1.

Table 1
Demographics and clinical characteristics of human brain tissues from acute traumatic brain injury and malignant glioma.

Case	Age	Gender	Cause of injury	Other injuries	Time post-injury (h)	Region of surgery	GCS
Traumatic brain injury	65	Male	Falling injury	None	7	Right parietal lobe	7
Traumatic brain injury	60	Female	Traffic accident	None	8	Right frontal lobe	7
Traumatic brain injury	66	Male	Falling injury	None	11	Right parietal lobe	6
Traumatic brain injury	70	Female	Traffic accident	None	8	Left frontal lobe	5
Traumatic brain injury	59	Male	Traffic accident	None	9	Left frontal lobe	6
Traumatic brain injury	73	Male	Traffic accident	None	10	Right parietal lobe	5
Malignant glioma	57	Male	-	None	-	Right parietal lobe	-
Malignant glioma	53	Female	-	None	-	Right parietal lobe	-
Malignant glioma	45	Female	-	None	-	Left parietal lobe	-
Malignant glioma	39	Male	-	None	-	Left frontal lobe	-

Animal TBI model

All animal protocols were conducted strictly in accordance with the National Institutes of Health Guide for the Care and Use of Laboratory Animals and approved by Tianjin Medical University Animal Care and Use committee. All C57BL/6 mice (6–8 weeks old and 20–25 g) were purchased from the Experimental Animal Laboratories of the Academy of Military Medical Sciences (Beijing, China). All mice were housed in a temperature (20℃–24℃) and humidity (50–60%) controlled environment with food and water available ad libitum under a standard 12 h light-dark cycle. TBI was conducted using a digital electromagnetically controlled cortical impact (CCI) device (eCCI-6.3 device, Custom Design & Fabrication, USA) as previously described [19]. Briefly, each mouse was anesthetized with 1–1.5% isoflurane in 30% oxygen and 70% nitrous oxide and subsequently placed prone in a stereotaxic head frame. An approximate 3.5-mm craniotomy was performed over the right parietal skull (2.5 mm posterior from the bregma and 2.5 mm lateral to the sagittal suture) using a motorized drill after exposing the skull using a

midline incision. A 4-mm flat-tip impactor was used to induce a unilateral 2.2 mm depth impact on the mouse cortex at 5 m/s speed with a 200 ms dwell time. Subsequently, the mice were placed into an incubator maintained at 37℃ to recover from the anesthesia. The sham-operated mice were only subjected to the same craniotomy without CCI infliction.

In vivo multiphoton microscopy

Intravital imaging was performed using an upright multiphoton laser-scanning microscope (Olympus Corporation, Shinjuku City, Tokyo, Japan) with an XL PLN 25X WMP dipping objective lens (Olympus). The emitted fluorescence was detected using a 495–540 nm filter. Mice were anesthetized with 1–1.5% isoflurane in 30% oxygen and 70% nitrous oxide and then placed prone on a heating plate (37 ± 0.5°C). After fixation on a custom head-fixing apparatus, a craniotomy was performed using a high-speed micro drill on the right cortex, located at a central position of 2.5 mm lateral and 1.5 mm posterior to the bregma [20]. The window of the right parietal skull was covered with sterile cover glass and fixed with dental cement. Cortex imaging was performed using a cranial window. To visualize the blood vessels, 0.1 ml FITC-dextran (2,000 kDa, Sigma-Aldrich, 10 mg/mL) was injected intravenously into the mice. The imaging depth was 200–400 μm from the brain surface. To detect neutrophils in cerebrovascular tissue, phycoerythrin (PE)-conjugated monoclonal Ly6G antibody (1A8 clone; 3 μg, 12-9668-80, eBioscience Inc., San Diego, California, United States) was injected intravenously into mice [20]. To visualize the NETs in the brain, 4 μL Sytox Green (S7020; 0.5 μL/ml, Invitrogen, Waltham, Massachusetts, United States) was injected intravenously into the mice 20 min before imaging.

Injection of adenoviruses

Recombinant PAD4 adenovirus (Adeno-PAD4; Adeno-CMV-Padi4-3*flag-tagged SV40-EGFP, 4×10^{10} plaque-forming-unit/mL) and empty adenovirus (Adeno-CMV-3*flag-tagged SV40-EGFP) were purchased from Genechem (Shanghai, China). A total of 4 μL of Adeno-PAD4 or Adeno-EGFP was stereotactically injected into two locations in the right cortex at a dose of 2 μL each 24 h before subjecting each mouse to CCI (1.5 mm caudal and 1.5 mm rostral from lesion epicenter). The injections were made at a depth of 1.0 mm using a 5 μL Hamilton syringe (Hamilton Company, USA) at a 0.5 μL/min flow rate through a hole [20, 21]. After the injection, the needle was maintained in the position for 10 min before retraction, and the scalp was sutured.

Neutrophil isolation and in vitro NET assay

Neutrophils were isolated from the femur and tibia of euthanized sham and TBI mice using a previously described protocol [22]. The bones were then cleaned with 75% ethanol and rinsed with ice-cold PBS. Bone marrow was flushed from the bones using an ice-cold buffer solution containing PBS, 0.5% bovine serum albumin (BSA), and 2 mM EDTA by diluting the MACS BSA stock solution (#130-091-376, Miltenyi Biotec, Germany) 1:20 with autoMACS Rinsing Solution (#130-091-222, Miltenyi Biotec, Germany). Bone marrow cells were centrifuged at 500 g for 5 min, followed by hypotonic lysis of the red blood cells. After washing twice with ice-cold buffer solution, the cells were incubated with Neutrophil Biotin-Antibody Cocktail (130-097-658, Miltenyi Biotec, Germany) and MicroBeads, and flow-through containing unlabeled

neutrophils was collected using a MACS Separator. Isolated neutrophils (5×10^5 cells/ml) were suspended in RPMI-1640 (Gibco, MA) and seeded in 48-well glass-bottomed plates in a 5% CO_2 incubator at 37℃ for 30 min before stimulation. As described previously [23], cells were treated with 10 μg/ml *Klebsiella pneumoniae* lipopolysaccharide (LPS, Sigma-Aldrich, MO, USA) at 37℃ for 2.5 h.

Enzyme-linked immunosorbent assay

Using Citrullinated Histone H3 enzyme-linked immunosorbent assay (ELISA) Kit (501620, Cayman Chemical Company, Ann Arbor, Michigan, United States), the levels of human S100A8/A9 (Cusabio, Wuhan, China), mouse MPO (Cusabio, Wuhan, China), human IFN-β (E-EL-H0085c, Elabscience, Wuhan, China), human IL-6 (E-EL-H0192c, Elabscience, Wuhan, China), mouse IFN-β (E-EL-M0033c, Elabscience, Wuhan, China), and mouse IL-6 (E-EL-M0044c, Elabscience, Wuhan, China) in serum or brain tissue were measured using commercially available ELISA kits following the manufacturer's instructions.

Quantification of NETs

Plasma was collected from the whole blood of mice and humans by centrifugation at 150 × *g* for 15 min. Plasma DNA was quantified according to the manufacturer's instructions using the Quant-iT PicoGreen dsDNA Assay kit (P11496, Invitrogen). We also developed a capture ELISA based on citrullinated histone H3 associated with DNA (H3cit-DNA complex), as reported previously [24]. Briefly, after overnight coating with anti-H3Cit (1:500, ab5103, Abcam, UK) at 4℃, 96-well plates were then blocked with 5% BSA for 2 h. After washing three times (300 μL), 50 μL of plasma or 60-fold dilution of the mouse brain tissue was added into the wells with 80 μL of incubation buffer containing a peroxidase-labeled anti-DNA mAb (Cell Death ELISA, 11774425001, Roche, Basel, Switzerland). The plates were then incubated at room temperature for 2 h. After five washes, the plate was developed with 100 μL ABST substrate. The absorbance (OD) at 450 nm was measured after 30 min incubation in the dark.

Neurological assessment

Neurological function was assessed using the modified neurological severity score (mNSS), as described previously [25]. Following TBI, the mNSS of mice was measured at 1, 3, 5, and 7 d. The mNSS consists of motor (muscular state and abnormal action), sensory (visual and tactile), reflex, and balance tests. A higher mNSS score represented more serious neurological deficits (normal score, 0; maximal score, 18). The assessment was performed by two individuals blinded to the group identity of each mouse.

Rotarod test

As described previously[26], the limb motor coordination and balance of mice were assessed using an accelerating Rota-rod apparatus (RWD Life Science, Shenzhen, China). Before induction of CCI, mice in each group were trained for three consecutive d. Then, at 1, 3, 5, and 7 d post-injury, each mouse was placed on the accelerating automated Rota-rod, which accelerated from 4 to 40 rpm/min within 5 min. The latency to fall for each mouse was recorded. Each mouse was tested three times with an interval of 30 min between trials, and the average latency to falling was used for analysis. The assessment was performed by two individuals blinded to the group identity of each mouse.

Neutrophil depletion

Mice received an intraperitoneal (i.p.) injection of 100 μg monoclonal anti-mouse Ly6G antibody (1A8 clone; specific for neutrophils, BE0075-1, BioXCell, NH) 24 h before TBI and 24 h after TBI. Control mice received 100 μg of the isotype antibody rat IgG2a in the same manner. The dose of anti-mouse Ly6G antibody and the administration interval was chosen based on a previous study [27].

Peptidyl arginine deiminases (PAD) inhibitor treatment

A stock solution of the PAD inhibitor, Cl-amidine (GC35706, GLPBIO, USA), was dissolved in dimethyl sulfoxide (DMSO) and diluted in saline (5% v/v). Then, 10 mg/kg Cl-amidine or vehicle (saline containing 5% DMSO) was administered i.p. once per day for three consecutive d beginning 10 min after TBI, as reported previously [18].

Human recombinant DNase 1 treatment

As previously reported [18], mice received an intravenous (i.v.) injection of 5 mg/kg rh DNase 1 (Deoxyribonuclease 1 human recombinant; enz-319-10,000 IU, ProSpec-Tany TechnoGene Ltd., Rehovot, Israel) or vehicle (8.77 mg/mL sodium chloride and 0.15 mg/mL calcium chloride) 1 h after TBI and then every day until the mice were euthanized.

2’3’-cGAMP treatment

As previously reported [23, 28], 1 mg/kg 2'3'-cGAMP (tlr-lnacga23-1; InvivoGen, San Diego, USA) or vehicle (phosphate-buffered saline, PBS) was administered intravenously 10 min before TBI; this was repeated 24 h and 48 h after TBI until the mice were killed.

Stimulators of interferon genes (STING) antagonist administration

The STING antagonist C-176 (S6575, Selleck, USA) was dissolved in a stock solution containing 5% dimethyl sulfoxide (DMSO) and 95% corn oil and then diluted in saline (5% v/v). As reported previously [29], 10 mg/kg C-176 or vehicle (saline containing 5% stock solution) was administered i.p. 1 h after TBI and then every day until the mice were killed.

Blood cell counts

Peripheral blood samples were obtained by puncturing the retro-orbital venous plexus from anesthetized mice three d after TBI. Blood samples were collected into 5 ml EDTA-containing tubes and analyzed using an SYSME X Hematology Analyzer (Sysme, Japan).

Cytospin NET analysis

Peripheral blood was collected from the retro-orbital venous plexus of the mice and lysed with red blood cell lysis buffer (Sigma-Aldrich, MO, USA). After washing, the cells were resuspended in 5% BSA in PBS for 1 h, followed by incubation with phycoerythrin (PE)-conjugated monoclonal Ly6G antibody (1A8 clone; 1

μg/ml, 12-9668-80, eBioscience) and Sytox Green (S7020; 0.5 μL/ml, Invitrogen) for 1 h. After washing three times, the cells were resuspended and plated on slides using Shandon Cytospin 4 (Thermo Scientific). Images were captured using an inverted fluorescence microscope (Olympus).

Western blotting

Brain tissue from the lesioned boundary of cortex and harvested cell pellets were immediately homogenized and lysed in RIPA lysis buffer (Sigma-Aldrich, MO, USA) containing protease and phosphatase inhibitor cocktails (Sigma-Aldrich, MO, USA) to obtain total protein. Equal amount of protein was suspended in loading buffer (denatured at 100℃ for 15 min) and were separated by sodium dodecyl sulfate-polyacrylamide gel electrophoresis (SDS-PAGE) and transferred to a 0.45um pore size polyvinylidene difluoride membranes (Millipore, Temecula, CA, USA). The membrane were blocked with 5% skimmed milk in Tris-buffered saline supplemented with 0.1% Tween-20 (TBST) for 2h at room temperature and incubated at 4℃ overnight with the following primary antibodies: rabbit anti-Histone H3 (anti-H3; 1:1000, 9715), rabbit anti-STING (1:1000, 13647), rabbit anti-cGAS (1:1000, 31659), rabbit anti-pTBK1 (1:1000, 5483), rabbit anti-TBK1 (1:1000,38066), rabbit anti-pIRF3 (1:1000, 4947), rabbit anti-IRF3 (1:1000, 4302),rabbit anti-pNF-κB (1:1000,3039), rabbit anti-NF-κB (1:1000,8242), rabbit anti-β-actin (1:2000, 4970, all from Cell Signaling Technology, MA), rabbit anti-H3Cit (1:1000, ab5103), rabbit anti-PAD4 (1:1000, ab96758, all from Abcam, UK), anti-Caspase1 (22915–1-AP, 1:2000, Proteintech Group, Wuhan, China), anti-GSDMD (AF4012, 1:2000, Affinity Biosciences), rat anti-Ly6G (1:1000, 551459, BD Pharmingen). The membranes were then washed with TBST and incubated with species-appropriate horseradish peroxidase (HRP)-labeled secondary antibodies (1:5000, Cell Signaling Technology, USA) for 1h at room temperature. Finally, the immunoblot bands were visualized under an imaging system (Bio-Rad, Hercules, CA, USA) and were qualified using Image Lab-5.2.1 software (Bio-Rad, CA, USA).

Immunofluorescence staining

The brains were removed and sliced into 8μm-thick coronal sections using a cryostat (Leica, Model CM1950, Germany). Sections were washed with PBS and permeabilized with 0.1% Triton X-100 (Sigma Aldrich) for 30 mins and incubated with 3% BSA for 1h at room temperature. Thereafter, sections were incubated overnight at 4℃ with primary antibodies, including rat anti-F4/80 (1:200, ab6640), goat anti-Iba1 (1:500, ab5076), rabbit anti-MPO (1:500, ab208670), goat anti-GFAP (1:200, ab53554) rabbit anti-H3Cit (1:1000, ab5103, all from Abcam, UK), rabbit anti-STING (1:500, 13647), rabbit anti-cGAS (1:200, 31659), anti-IL-6 (1:200, 12912, all from Cell Signaling Technology), goat anti-CD31 (1:200, AF806), goat anti-CD31

(1:200, AF3628), goat anti-MPO (1:500, AF3667, all from R&D Systems), rat anti-mouse Ly6G (1:200, 551459, BD Biosciences), rat anti-mouse CD16/32(1:500, 553142, BD Biosciences), mouse anti-TNF-α (1:500, 60291–1-Ig, Proteintech Group, Wuhan, China), mouse anti-Caspase1 (1:500, sc-56036, Santa Cruz Biotechnology). The sections were then incubated with the species-appropriate Alexa Fluor-conjugated IgG (1:500, Invitrogen, USA) for 1h at room temperature. DNA was stained with 4’,6-diamidino-2-phenylidole (DAPI, Abcam). Staining was visualized and captured by an inverted fluorescence

microscope (Olympus, Japan). For each animal, three fields from lesioned boundaries of cortex in each section were digitized under x40 objective. Images were analyzed using ImageJ software (Version 1.46r, Wayne Raband, USA).

Immunohistochemistry staining

Immunohistochemistry staining was performed as previously described[30]. Deparaffinized sections (8μm) were incubated with 0.3% hydrogen peroxide (H_2O_2) for 15 min to block endogenous peroxidase, and then incubated with 5% BSA for 1 h at room temperature. Thereafter, sections were incubated overnight at 4℃ with primary antibodies, including rabbit anti-H3Cit (1:1000, ab5103), rabbit anti-MPO (1:1000, ab208670), rabbit anti-GSDMD (1:500, ab219800, all from Abcam, UK), rabbit anti-Iba1 (1:1000, 17198), rabbit anti-CD86 (1:500, 19589, all from Cell Signaling Technology, MA). The sections were washed with PBS and then incubated with HRP-conjugated goat anti-rabbit secondary antibodies for 1h. Finally, the immunoreactivity was visualized with 3,3’-diaminobenzidine (DAB, ZLI-9017, ZSGB-Bio). All slides were captured using a Nikon light microscope (Nikon, Tokyo, Japan).

Quantitative real-time polymerase chain reaction (qPCR) analysis

Total RNA was extracted from homogenized lesion boundary of cortex using Trizol regent (Invitrogen, Thermo fisher scientific) and cDNA was synthesized from 2ug RNA using PrimeScript RT Reagent Kit (Takara Bio, Tokyo, Japan). The PCR assays were performed on a Real-Time PCR Detection System (Bio-Rad, Hercules, CA, USA) using SYBR Green PCR Master Mix (Applied Biosystems, Waltham, MA, USA). The relative gene expression levels were normalized to GAPDH.

Quantitative real-time polymerase chain reaction (qPCR) analysis

Total RNA was extracted from the homogenized lesion boundary of the cortex using Trizol regent (Invitrogen, Thermo fisher scientific) and cDNA was synthesized from 2ug RNA using PrimeScript RT Reagent Kit (Takara Bio, Tokyo, Japan). The PCR assays were performed on a Real-Time PCR Detection System (Bio-Rad, Hercules, CA, USA) using SYBR Green PCR Master Mix (Applied Biosystems, Waltham, MA, USA). The relative gene expression levels were normalized to GAPDH. The primers used in this study are shown in Table 2.

Table 2
Primers used for quantification of mRNA expression in brain by RT-qPCR

Gene	Sequences of primer (5'to 3')
IFN-β	GCCCTCTCCATCAACTATAAGCAG
	CAACAATAGTCTCATTCCACCCAGT
IL-18	AGGATGAAAATGGGGATAAATCTGT
	AGCCTCGGGTATTCTGTTATGGA
iNOs	GGAGCGAGTTGTGGATTGT
	GTGGGAGGGGTCGTAATG
IL-6	CTCCCAACAGACCTGTCTATAC
	CCATTGCACAACTCTTTTCTCA
IL-1β	GCGCTGCTCAACTTCATCTTG
	GTGACACATTAAGCGGCTTCAC
TNF-α	GTGACAAGCCTGTAGCCCA
	ACTCGGCAAAGTCGAGATAG
GAPDH	AATGTGTCCGTCGTGGATCTGA -
	GATGCCTGCTTCACCACCTTCT

Statistical analysis

All statistical analysis was performed with Graph-Pad Prism software (Graph Pad Software, Version8.1.2 San Diego, CA, USA). Multiple comparisons were analyzed by one-way analysis of variance (ANOVA) followed by Tukey's multiple comparison post hoc test. The results were expressed as means ± (SD). Comparison between 2 groups was performed by unpaired Student's t-test or Mann-Whitney test. A value of $P < 0.05$ was considered statistically significant.

Results

Neutrophils infiltrate the cerebral parenchyma around the contusion area in patients with TBI.

To detect whether neutrophils are present in the brain parenchyma of TBI patients, we obtained brain specimens from six TBI patients who underwent a decompressive craniotomy to remove the hematoma and/or to reduce life-threatening high intracranial pressure. Control brain specimens were obtained from four patients with glioma who underwent maximizing resection of malignant glioma to improve survival. Hematoxylin and eosin staining indicated the presence of neutrophils in the cerebral parenchyma around the contact brain areas (Fig. 1a). Immunostaining showed a significant increase in the total neutrophil

MPO content in contusion areas after TBI (Fig. 1b). Double immunofluorescence staining showed that MPO-positive neutrophils broadly accumulated in the injured CD31-positive blood vessels and infiltrated into the extravascular brain parenchyma (Fig. 1c).

Neutrophils infiltrate peri-injury regions and promote microglia/macrophage activation and M1 polarization in mice with TBI

We subjected the mice to TBI and analyzed the brain cortexes at 1 h, 3 h, 6 h, 12 h, 1 d, 3 d, 5 d, 7 d, and 14 d. Using an anti-lymphocyte antigen 6 complex locus G (Ly6G) antibody, we found that the neutrophil level in the ipsilateral cerebral cortex increased in a time-dependent manner compared to sham mice, reaching the peak level at 3 d after TBI and persisting at 14 d post-injury (Fig. 2b, c). We then detected a significant increase in MPO protein levels in the contused cortex of mice 3 d after TBI (Fig. 2d). Immunostaining showed that MPO-positive neutrophils increased significantly throughout the cortical contusion areas 3 d post-injury. However, there was no significant change in sham-operated mice (Fig. 2e). Neutrophils were found inside the CD31-positive blood capillaries, and extravascular brain parenchyma (Fig. 2f). *In vivo* multiphoton microscopy showed that numerous Ly6G-labeled neutrophils were aggravated and adhered to blood vessels and infiltrated into the extravascular brain parenchyma at 3 d. In contrast, neutrophils were barely detectable in the sham-operated mice (Fig. 2g). We also detected a higher neutrophil count (Fig. 2h) and a higher percentage of peripheral blood neutrophils (Fig. 2i) at 3 d after TBI, as analyzed using a SYSME X Hematology Analyzer.

Neutrophil migration into the parenchyma contributes to microglial activation by releasing ROS, lipocalin, and MMP9[5]. To investigate the effect of neutrophils on microglial activation and M1 polarization, we intravenously used an anti-Ly6G antibody to deplete neutrophils in mice for 3 d. Peripheral blood counts showed a 37.2% reduction in the number of blood neutrophils in anti-Ly6G-treated mice compared to that in isotype-treated mice **(Figure S1a).** We also found that the ratio of neutrophil to leukocyte in the neutrophil-depleted mice was significantly decreased compared to that in isotype-treated mice at 3 d after TBI **(Figure S1b)**. In contrast, the total number of leukocytes was unchanged (**Figure S1c)**. Consistently, immunostaining showed that the number of infiltrated neutrophils in the lesioned boundaries of the cortex was significantly lower in anti-Ly6G-treated mice than in isotype-treated mice (Fig. 3a). Then, we found that anti-Ly6G treatment effectively improved neurological deficits in mice at 3 d after TBI (Fig. 3b, c). Immunostaining showed that the number of astrocytes around the injured area did not change significantly (Fig. 3d). However, the number of migrating microglia/macrophages around the injured area decreased by 44.0% in anti-Ly6G-treated mice when compared to isotype-treated mice (Fig. 3e, f). We tested the role of neutrophil infiltration in microglial M1 polarization and pyroptosis using immunofluorescence staining. The results showed that the number of CD16/32 positive microglia/macrophages in the peri-contusion region was significantly increased 3 d after TBI compared with the sham-operated brain (Fig. 3g, h). Mice administered with anti-Ly6G antibody showed a 30.8% reduction in the number of M1 phenotype microglia/macrophages in the peri-contusion region when

compared to mice treated with an isotype. We also found that the number of caspase-1 positive microglia in the lesioned boundaries of the cortex was significantly increased 3 d after TBI (Fig. 3i, j). In contrast, treatment with anti-Ly6G antibody significantly reduced the number of pyroptotic microglia/macrophages. In line with this, an increased number of IL-6-positive microglia/macrophages (Fig. 3k, l) and TNF-α-positive microglia/macrophages (Fig. 3m, n) were also significantly reversed by the anti-Ly6G antibody in mice subjected to TBI.

TBI induces neutrophil extracellular trap formation

A recent study confirmed that NETs circulated in the peripheral blood of TBI patients and correlated with the Glasgow Coma Scale (GCS) score and ICP[18]; however, whether NETs reach the brain parenchyma after TBI remains unknown. Consistent with these findings, we first detected a significantly elevated neutrophil number in patients with TBI by examining Wright-stained peripheral blood smears (Fig. 4a-c). Additionally, we also found several nuclear envelope-disassembled neutrophils and extracellular DNA formation in blood smears from patients with TBI (Fig. 4b). According to a previous study, this pathological alteration is termed NETosis [15], and the number of these pathological alterations is significantly increased in the blood smears of patients with TBI (Fig. 4d). Importantly, neutrophil and neutrophil-derived NETs were readily found in injured brain tissue from TBI patients with double immunofluorescence staining of MPO and NETs specific markers (citrullinated histone H3, H3cit) (Fig. 4e, f). Consistently, immunostaining showed that the number of H3cit-positive cells in injured brain tissue from patients with TBI was significantly increased (Fig. 4g). Hematoxylin and eosin staining clearly showed that extracellular DNA fibers were present in the contused brain tissue from patients with TBI (Fig. 4h).

Next, we aimed to investigate whether neutrophil-released NETs are present in the circulation and peri-contusion of TBI mice and whether they affect microglia-mediated inflammatory responses. First, we found that the circulating DNA and H3cit-DNA complex levels were significantly elevated in the plasma of TBI mice when compared to sham-operated mice (Fig. 5a, b). Consistently, cytospin revealed that the numbers of neutrophils and Sytox-positive neutrophils in peripheral blood from TBI mice increased significantly, indicating that the levels of NETosis in peripheral blood were significantly upregulated in TBI mice compared to those in sham-operated mice (Fig. 5c-e). We isolated neutrophils from the bone marrow of mice and stimulated them with or without lipopolysaccharide (LPS). We detected that both unstimulated and LPS-stimulated neutrophils from TBI mice showed a significant increase in H3cit positive neutrophils and NET formation (Fig. 5f–h), indicating that neutrophils from TBI mice are more sensitive to stimulation and primed to promote NETosis. Consistent with the patient study, the expression of H3cit in the ipsilateral cortex increased in a time-dependent manner compared to that in sham-operated mice, reaching the peak level at 3 d and persisting for at least 14 d after TBI (Fig. 5i, j). ELISA analysis showed a marked 1.21-fold increase in the total content of the DNA-H3cit complex in the cortical homogenates from TBI mice compared to sham-operated mice (Fig. 5k). Hematoxylin and eosin staining clearly showed that DNA fibers were present in the contused cortex at 3 d post-injury (Fig. 5l). Immunofluorescence staining showed that NETs marker H3cit positive neutrophils in these areas were

also abundantly present at 3 d (Fig. 5m). To validate these observations shown by histological analyses, we detected NET formation in peri-contusions using an *in vivo* multiphoton microscope. The results revealed that Sytox green-labeled neutrophil extracellular DNA fibers were extensively observed around the contused cortex 3 d after TBI, while these fibers were not detected in the nontraumatic cortex (Fig. 5n).

Levels of circulating NET correlate with levels of plasma cGAS-STING pathway activation in the peripheral blood of patients with TBI.

Previous studies have confirmed that extracellular double-stranded DNA (dsDNA) is one of the most critical components of NETs [31] and is tightly monitored and sensed by DNA-sensing pattern recognition receptors, among which cGAS is currently defined as a critical DNA-sensing receptor [32]. Subsequently, we measured the levels of circulating NET markers and STING-related IFN-β and IL-6 in the peripheral blood of TBI patients. ELISA analysis suggested that the levels of plasma DNA (Fig. 6a), DNA-H3cit complex (Fig. 6b), plasma H3cit (Fig. 6c), and plasma S100A8/A9 (Fig. 6d) were all markedly increased in peripheral blood among TBI patients compared with matched healthy donors. This indicated that the level of circulating NET formation in peripheral blood from TBI patients was higher than that in healthy donors. The levels of STING-related IFN-β and IL-6 in the peripheral blood of TBI patients were also quantified using ELISA, and the results suggested that the levels of IFN-β (Fig. 6e) and IL-6 (Fig. 6f) were significantly elevated in the peripheral blood of TBI patients compared to healthy donors, indicating that the cGAS-STING pathway may be upregulated in the central nervous system and/or peripheral blood after TBI. We then used Spearman correlation analysis to investigate whether circulating NET marker levels correlated with levels of plasma STING-related IFN-β and IL-6. Intriguingly, all plasma NET marker levels positively correlated with levels of plasma STING-related IFN-β (Fig. 6g, i, k, m) and IL-6 (Fig. 6h, j, l, n) in peripheral blood from TBI patients, indicating that circulating NET formation may promote activation of the cGAS-STING pathway in the central nervous system and/or peripheral blood after TBI. Subsequently, we measured the protein expression of cGAS and STING in the cortex at 6 h, 12 h, 1 d, 3 d, 5 d, 7 d, and 14 d after TBI (Fig. 6o). We found elevated levels of cGAS (Fig. 6p) and STING (Fig. 6q), which peaked at 3 d in mice subjected to TBI. In addition, double immunofluorescence staining was performed on brain sections to identify the type of cells expressing cGAS and STING in the brain 3 d after TBI. We observed prominent cGAS (Fig. 6r) and STING (Fig. 6s) staining in Iba-1 positive microglia cells and F4/80 positive macrophages, with only slight staining in GFAP-positive astrocytes, but almost no staining in Ly6G positive neutrophils and CD31 positive endothelial cells. These observations validated our hypothesis that NETs contribute to microglia/macrophages activation via the cGAS-STING pathway after TBI.

Degradation of NETs-associated DNA ameliorates activation and M1 polarization of microglia/macrophages by inhibiting the cGAS-STING pathway

We next validated whether the degradation of NET-associated DNA with DNase 1 could ameliorate activation and M1 polarization of microglia/macrophages via the cGAS-STING pathway. Immunofluorescence staining showed that the number of cGAS-positive microglia/macrophages significantly increased in the peri-contusion cortex of TBI mice compared to that in sham-operated mice

(Fig. 7a, b). Treatment with DNase 1 significantly reduced the number of cGAS-positive microglia/macrophages (Fig. 7a, b). This effect of DNase 1 was abolished in mice that also received the DNA sensor cyclic GMP-AMP (cGAMP) 3 d after TBI (Fig. 7a, b). In line with this finding, the amounts of STING-positive microglia/macrophages in the peri-contusion cortex were also significantly reduced by DNase 1 treatment. In contrast, cGAS product cGAMP treatment also reversed the effect of DNase 1 (Fig. 7c, d). We subsequently found that the expression of STING, TANK-binding kinase 1 (TBK1), IFN regulatory factor 3 (IRF3), and IFN-β and IL-6 induction was upregulated in the cortex of mice subjected to TBI (Fig. 7e-j). DNase 1 treatment significantly rescued the activation of the cGAS-STING pathway and production of IFN-β and IL-6(Fig. 7e-j). However, treatment with the cGAS product cGAMP effectively reversed the effect of DNase 1 on the activation of the cGAS-STING pathway and the production of IFN-β and IL-6(Fig. 7e-j). We also found that DNase 1 treatment significantly reduced the number of CD86-positive cells and GSDMD-positive cells in the lesioned cortex 3 d after TBI, while an infusion of cGAMP significantly abolished the effects of DNase 1(Fig. 7k-n). Double immunofluorescence staining showed that the number of caspase-1-positive microglia/macrophages in the cortex of TBI mice was significantly higher than that in the sham-operated mice. Compared with the vehicle controls, treatment with DNase 1 significantly reduced caspase-1 positive microglia /macrophages 3 d after TBI (Fig. 7o, p). However, infusion of cGAMP significantly reversed the inhibitory effect of DNase 1 on TBI-induced increase in microglia/macrophage pyroptosis (Fig. 7o, p). Consistent with these data, western blot analysis showed that the protein levels of NF-κB and iNOs were significantly upregulated in the cortex at 3 d in mice with TBI compared to sham-operated mice (Fig. 7q-s). We also found that DNase 1 treatment significantly inhibited the activation of the NF-κB signaling pathway and M1 phenotype microglia/macrophages, while an infusion of cGAMP significantly reversed the effects of DNase 1(Fig. 7q-s). These results indicate that degradation of neutrophil-released NETs associated DNA with DNase 1 could reduce the amounts of M1-like phenotype microglia/macrophages and pyroptotic microglia/macrophages in peri-contusion areas after TBI, primarily via the cGAS-STING pathway.

PAD4 promotes M1 phenotype microglia/macrophage activation and microglia/macrophage pyroptosis through the cGAS-STING pathway.

Peptidylarginine deiminase 4 (PAD4) is a histone-modifying enzyme that plays a key role in NET formation[33]. To test the hypothesis that increased formation of NET, orchestrated by PAD4, participated in microglia/macrophage-mediated inflammation after TBI, we first studied the role of overexpression of PAD4 on microglia/macrophage activation and pyroptosis in mice with TBI. Immunoblotting showed marked 14.6-fold upregulation of PAD4 protein expression and 2.88-fold upregulation of H3Cit protein expression in the contused cortex at 3 d after injection of PAD4 adenovirus when compare with control virus in mice with TBI (Fig. 8a-c), indicating NET formation increased after injection of PAD4 adenovirus. Immunohistochemical analysis also showed extensive expression of recombinant adeno-PAD4-EGFP-infected cells in the cortex 3 d after injection (Fig. 8d). Immunofluorescence staining showed that administration of PAD4 adenovirus into the cortex caused a significant increase in the number of STING-positive microglia/macrophage when compared with control virus in mice with TBI (Fig. 8e, f). However, this effect of PAD4 adenovirus was rescued in mice that also received STING inhibitor C-176 (Fig. 8e, f).

We consistently found that the protein levels of STING, TBK1, and IRF3 and the mRNA levels of IFN-β and IL-6 in the cortex were significantly upregulated in TBI mice infected with PAD4 adenovirus (Fig. 8g-l). However, the increase in the expression of proteins associated with the cGAS-STING pathway and mRNA expression of IFN-β and IL-6, amplified by PAD4 adenovirus, was rescued by STING inhibitor C-176 (Fig. 8g-l). Moreover, the numbers of pro-inflammatory M1 phenotype microglia/macrophage and pyroptotic microglia/macrophage were also increased in the contused cortex 3 d after PAD4 adenovirus injection (Fig. 8m-p). However, this pro-inflammatory effect of PAD4 adenovirus in the contused cortex was effectively inhibited by C-176 (Fig. 8m-p). Consistently, administration of PAD4 adenovirus significantly increased the protein expression of NF-κB and mRNA expression of iNOs, TNF-α, IL-1β, and IL-18 in the peri-contusion cortex, while an injection of C-176 significantly abolished the pro-inflammatory effects of PAD4 adenovirus (Fig. 8q-v). However, there was no significant difference in mNSS and the Rotarod test between control mice and PAD4-overexpressing mice (Fig. 8w, x), indicating cortical localized injection of PAD4 adenovirus was not aggravated neurological deficits. Notably, compared with PAD4-overexpressing mice, PAD4-overexpressing mice combined with an intraperitoneal injection of C-176 showed better neurological performance (Fig. 8w, x).

To further investigate the role of NETs in microglia/macrophage activation, we compared vehicle-treated mice with mice treated with the PAD inhibitor Cl-amidine after TBI. Immunofluorescence staining showed that treatment with Cl-amidine significantly reduced the number of STING-positive microglia/macrophages (Fig. 9a, b). This effect was blocked in mice that also received cGAMP after TBI (Fig. 9a, b). Consistently, we found that the expression of STING, TBK1, and IRF3 and the production of IFN-β and IL-6 in the cortex was significantly reduced in TBI mice treated with Cl-amidine (Fig. 9c-h). However, the decrease in the expression of proteins associated with the cGAS-STING pathway, rescued by Cl-amidine, was reversed by cGAMP (Fig. 9c-h). Moreover, Cl-amidine treatment significantly reduced the number of CD16/32-positive microglia/macrophages in the peri-contusion cortex, while an infusion of cGAMP significantly abolished the effects of Cl-amidine (Fig. 9i, j). We also found that the number of caspase-1-positive microglia/macrophages in the contused cortex was significantly lower in Cl-amidine-treated mice than in vehicle-treated mice three d after TBI (Fig. 9k, l). We also observed that cGAMP partly abolished the Cl-amidine-mediated decrease in microglia/macrophage pyroptosis in TBI mice (Fig. 9k, l). Consistent with these data, western blot analysis showed that the protein levels of NF-κB, caspase-1, and GSDMD were significantly upregulated in the cortex at 3 d in mice with TBI compared to sham-operated mice (Fig. 9m-q). Cl-amidine-treated TBI mice showed significantly reduced expression of these proteins compared with TBI mice receiving vehicle buffer, whereas cGAMP reversed the protective effect of Cl-amidine (Fig. 9m-q). Similar results also showed that the administration with Cl-amidine after TBI markedly suppressed the mRNA level of M1 pro-inflammatory cytokines (IL-1β, TNF-α, and IL-6) in the injured cortex, while the anti-inflammatory effect of Cl-amidine was significantly abolished when combined with cGAMP (Fig. 9r-t). In parallel with and effects on cerebral inflammatory responses, PAD4 inhibition with Cl-amidine improved neurological deficits as assayed by the mNSS and the Rotarod test, whereas cGAMP reversed the neuroprotective effect of Cl-amidine. Collectively, these data suggest that

PAD4 regulates M1 microglia/macrophage activation and microglia/macrophage pyroptosis primarily through cGAS.

Discussion

Among patients with acute TBI, microglia are the major innate immune cells that respond within minutes by moving toward the areas with damage and can be sustained for many years [34]. Microglia, the major cellular component of the innate immune system in the central nervous system (CNS), reportedly plays a critical role in neuronal death, blood-brain barrier disruption, brain edema, cerebrovascular dysfunction, and neurological deficits after TBI [35, 36]. In addition, with the breakdown of the blood-brain barrier and chemokines released by activated microglia, large amounts of neutrophils from the peripheral immune system mobilize inside the cerebral blood vessels and infiltrate the brain parenchyma, leading to vascular destruction and aggravation of intracranial immune inflammatory responses [5].

While previous studies have shown that massive neutrophil infiltration into the cerebral parenchyma can directly interact with microglia using intravital intracranial two-photon microscopy in a mouse model of stroke [10, 11], no direct evidence indicates that neutrophils affect the subpopulation of microglia and microglia-mediated inflammatory responses in TBI [5]. This is the first study to demonstrate that neutrophils are present in the brain parenchyma of TBI patients and that neutrophil depletion ameliorates microglia/macrophage activation-mediated intracranial inflammatory responses in a mouse model of TBI. Furthermore, we identified NETs released by neutrophils as distinct mediators of the mechanisms that promote M1 phenotypic and pyroptotic microglia/macrophages after TBI. We further found that the cGAS-STING pathway participates in NET-mediated effects on neutrophil-associated microglial inflammatory responses after TBI.

A previous clinical study reported a marked increase in peripheral neutrophils in the early hours after TBI that lasted until 48 h post-injury [37]. Following the disruption of the blood-brain barrier (BBB) and activation of CNS resident immune cells, neutrophils are usually among the first peripheral immune cells to reach the contused brain and do so in just a few hours [38, 39]. Consistently, we found that the number of neutrophils in the peripheral blood and peri-contusion cortex in mice significantly increased 3 d after TBI. Brain sections of patients with TBI also showed that massive numbers of neutrophils reached the contused brain area, accumulated in the blood vessels, and infiltrated into the parenchyma. With increasing interest in examining the correlation between peripheral and cerebral inflammatory responses after TBI, it has been clarified that while neutrophil infiltration is one of the earliest inflammatory responses, a pronounced microglial/macrophage response develops in the subacute phase post-injury [34]. A previous study demonstrated that neutrophil depletion reduced microglial/macrophage responses and ameliorated brain edema 7 d after TBI [6]. Consistent with those findings, we found that after neutrophil depletion, the amounts of M1 phenotypic microglia/macrophages and pyroptotic microglia/macrophages in the peri-contusion cortex reduced significantly 3 d after injury. However, a previous study showed that anti-integrin therapies could induce progressive multifocal

leukoencephalopathy in patients with multiple sclerosis [40], and it remains unclear whether long-term neutrophil depletion can induce side effects.

NETs, which consist of extracellular DNA combined with histones, neutrophil elastase, and MPO, are released by neutrophils and form traps to kill pathogens [15]. However, growing evidence suggests that dysfunction of the inhibitory mechanism of NET and excess NET yield are also prominent pathogenic mechanisms that may lead to disease [15]. A recent study reported that NET formation correlated with elevated ICP and worse neurological function in patients with TBI [18]. In the present study, we first found that NET forms in the peripheral blood and contused brain in patients with TBI. We then reported that neutrophils isolated from TBI mice had more spontaneous NETs and showed greater sensitivity to promote NET formation after stimulation with LPS. Degradation of NETs with DNase 1 significantly inhibits microglia/macrophage-mediated inflammatory responses and microglia/macrophages pyroptosis in TBI mice, indicating that NET formation may be a potential mechanism by which neutrophils aggravate microglia-mediated cerebral inflammation post-trauma. This result is consistent with previous observations in mice with SAH where digestion of NETs with DNase 1 effectively inhibited the pro-inflammatory phenotype transition of microglia/macrophages and pyroptotic microglia/macrophages [41].

PAD4, a key enzyme in chromatin decondensation during NET formation [42], was markedly upregulated in the cortex 3 d after TBI. Inhibition of NET formation by PAD4 pharmacological inhibitor significantly weakens the inflammatory responses caused by M1 phenotypic microglia/macrophages and pyroptotic microglia/macrophages in mice with TBI. Conversely, overexpression of PAD4 in the cortex following stereotactic adenoviruses injection could aggravate microglia/macrophage-mediated cerebral inflammatory responses after TBI. These results revealed that NET formation, mediated by PAD4, is critical in regulating microglia/macrophage-mediated neuroinflammation and recovery of neurological functions after TBI.

Previous studies have demonstrated that the cGAS-STING pathway is a major cytosolic DNA sensor and plays a vital role in the microglial activity and neuroinflammatory responses after TBI [29, 43, 44]. Consistently, our results showed that TBI led to the upregulation of STING, activation of TBK1 and IRF3, and induction of STING-associated IFN-β and IL-6. Furthermore, we found that the degradation of NETs or inhibition of NET formation effectively suppressed the activation of the cGAS-STING pathway in microglia/macrophages and the production of IFN-β and IL-6, whereas the cGAS product cGAMP reversed these protective effects. We also observed that the overproduction of NETs by adenoviruses amplified the activation of the cGAS-STING pathway in microglia/macrophages and the synthesis of IFN-β and IL-6, exacerbating microglia/macrophage-mediated neuroinflammation after TBI. Notably, treatment with the STING inhibitor C-176 effectively blocked the pro-inflammatory phenotypic transition of microglia/macrophages and pyroptotic microglia/macrophages. These results suggest that cGAS-STING pathway activation predominantly mediates microglia/macrophage-associated neuroinflammatory responses aggravated by NETs following TBI.

Conclusion

The data obtained from our study demonstrated that TBI led to neutrophil accumulation in the contused brain, releasing detrimental signals, such as NETs, which subsequently promoted neuroinflammation by enhancing M1 microglia/macrophage polarization and priming microglia/macrophage pyroptosis. Crucially, we revealed that activation of the cGAS-STING pathway largely participates in NET-mediated effects on neutrophil-associated microglia/macrophage inflammatory responses after TBI. Considered together, our results highlight that targeting NETs is a promising therapeutic strategy for TBI treatment.

Declarations

Ethics approval and consent to participate

Each study participant or their Legal Authorized Representative gave written informed consent for study enrollment in accordance with the Declaration of Helsinki. Human tissue was obtained in accordance with an ethically reviewed and approved protocol from Tianjin Medical University General Hospital (IRB2020-WZ-162). All experimental procedures were conducted in accordance with the National Institutes of Health Guide for the Care and Use of Laboratory Animals and approved by Tianjin Medical University Animal Care and Use committee. All procedures were approved by the Chinese Small Animal Protection Association Experimental Protocol.

Consent for publication

Not applicable

Availability of data and materials

The datasets generated and analyzed during the current study are available from the corresponding author upon reasonable request.

Abbreviations

TBI, traumatic brain injury; NET, neutrophil extracellular trap; PAD4, peptidylarginine deiminase 4; ROS, reactive oxygen species; MPO, myeloperoxidase; GCS, Glasgow coma scale; CCI, controlled cortical impact; BSA, bovine serum albumin; ELISA, enzyme-linked immunosorbent assay; mNSS, modified neurological severity score; STING, Stimulators of interferon genes; SDS-PAGE, sodium dodecyl sulfate-polyacrylamide gel electrophoresis; LPS, lipopolysaccharide; qPCR, quantitative real-time polymerase chain reaction; CNS, central nervous system; BBB, blood-brain barrier.

Competing interests

The authors declare that they have no competing interests.

Funding

This work was supported by grants from the National Natural Science Foundation of China (no. 81930031, 81720108015, 81901525, 81801234, and 82071389), the Natural Science Foundation of Tianjin (No.19JCQNJC09500), the Science & Technology Development Fund of Tianjin Education Commission for Higher Education (No. 2019ZD034) and the Science & Technology Development Fund of Tianjin (NO.22JRRCRC00020).

Authors' contributions

S.Z, JN.Z. designed the experiment; MM.S, L.L, YY.C, XB.M, FL.C, T.L, and HR.J performed most of the experiments; L.M, XL.L, Y.Z, SH.L, GL.Y, YF.Z assisted in data analysis; X.L, QJ.D, X.C. wrote the manuscript; S.Z, JN.Z. provided the overall guidance.

Acknowledgments

Not applicable

References

1. Collaborators GBDN: **Global, regional, and national burden of neurological disorders, 1990–2016: a systematic analysis for the Global Burden of Disease Study 2016**. Lancet Neurol 2019, **18**(5):459–480.
2. Willis EF, MacDonald KPA, Nguyen QH, Garrido AL, Gillespie ER, Harley SBR, Bartlett PF, Schroder WA, Yates AG, Anthony DC *et al*: **Repopulating Microglia Promote Brain Repair in an IL-6-Dependent Manner**. Cell 2020, **180**(5):833–846 e816.
3. Hickman S, Izzy S, Sen P, Morsett L, El Khoury J: **Microglia in neurodegeneration**. Nat Neurosci 2018, **21**(10):1359–1369.
4. Erturk A, Mentz S, Stout EE, Hedehus M, Dominguez SL, Neumaier L, Krammer F, Llovera G, Srinivasan K, Hansen DV *et al*: **Interfering with the Chronic Immune Response Rescues Chronic Degeneration After Traumatic Brain Injury**. J Neurosci 2016, **36**(38):9962–9975.
5. Liu YW, Li S, Dai SS: **Neutrophils in traumatic brain injury (TBI): friend or foe?** J Neuroinflammation 2018, **15**(1):146.
6. Kenne E, Erlandsson A, Lindbom L, Hillered L, Clausen F: **Neutrophil depletion reduces edema formation and tissue loss following traumatic brain injury in mice**. J Neuroinflammation 2012, **9**:17.
7. Drummond RA, Swamydas M, Oikonomou V, Zhai B, Dambuza IM, Schaefer BC, Bohrer AC, Mayer-Barber KD, Lira SA, Iwakura Y *et al*: **CARD9(+) microglia promote antifungal immunity via IL-1beta- and CXCL1-mediated neutrophil recruitment**. Nat Immunol 2019, **20**(5):559–570.
8. Li Y, Ritzel RM, Khan N, Cao T, He J, Lei Z, Matyas JJ, Sabirzhanov B, Liu S, Li H *et al*: **Delayed microglial depletion after spinal cord injury reduces chronic inflammation and neurodegeneration in the brain and improves neurological recovery in male mice**. Theranostics 2020, **10**(25):11376–11403.

9. Loane DJ, Kumar A: **Microglia in the TBI brain: The good, the bad, and the dysregulated**. Exp Neurol 2016, **275 Pt 3**:316–327.
10. Neumann J, Riek-Burchardt M, Herz J, Doeppner TR, Konig R, Hutten H, Etemire E, Mann L, Klingberg A, Fischer T *et al*: **Very-late-antigen-4 (VLA-4)-mediated brain invasion by neutrophils leads to interactions with microglia, increased ischemic injury and impaired behavior in experimental stroke**. Acta Neuropathol 2015, **129**(2):259–277.
11. Neumann J, Henneberg S, von Kenne S, Nolte N, Muller AJ, Schraven B, Gortler MW, Reymann KG, Gunzer M, Riek-Burchardt M: **Beware the intruder: Real time observation of infiltrated neutrophils and neutrophil-Microglia interaction during stroke in vivo**. PLoS One 2018, **13**(3):e0193970.
12. Schauer C, Janko C, Munoz LE, Zhao Y, Kienhofer D, Frey B, Lell M, Manger B, Rech J, Naschberger E *et al*: **Aggregated neutrophil extracellular traps limit inflammation by degrading cytokines and chemokines**. Nat Med 2014, **20**(5):511–517.
13. Dwivedi N, Radic M: **Citrullination of autoantigens implicates NETosis in the induction of autoimmunity**. Ann Rheum Dis 2014, **73**(3):483–491.
14. Sharma S, Hofbauer TM, Ondracek AS, Chausheva S, Alimohammadi A, Artner T, Panzenboeck A, Rinderer J, Shafran I, Mangold A *et al*: **Neutrophil extracellular traps promote fibrous vascular occlusions in chronic thrombosis**. Blood 2021, **137**(8):1104–1116.
15. Papayannopoulos V: **Neutrophil extracellular traps in immunity and disease**. Nat Rev Immunol 2018, **18**(2):134–147.
16. Denorme F, Portier I, Rustad JL, Cody MJ, de Araujo CV, Hoki C, Alexander MD, Grandhi R, Dyer MR, Neal MD *et al*: **Neutrophil extracellular traps regulate ischemic stroke brain injury**. J Clin Invest 2022, **132**(10).
17. Laridan E, Denorme F, Desender L, Francois O, Andersson T, Deckmyn H, Vanhoorelbeke K, De Meyer SF: **Neutrophil extracellular traps in ischemic stroke thrombi**. Ann Neurol 2017, **82**(2):223–232.
18. Vaibhav K, Braun M, Alverson K, Khodadadi H, Kutiyanawalla A, Ward A, Banerjee C, Sparks T, Malik A, Rashid MH *et al*: **Neutrophil extracellular traps exacerbate neurological deficits after traumatic brain injury**. Sci Adv 2020, **6**(22):eaax8847.
19. Shi M, Mi L, Li F, Li Y, Zhou Y, Chen F, Liu L, Chai Y, Yang W, Zhang J *et al*: **Fluvoxamine Confers Neuroprotection via Inhibiting Infiltration of Peripheral Leukocytes and M1 Polarization of Microglia/Macrophages in a Mouse Model of Traumatic Brain Injury**. J Neurotrauma 2022, **39**(17–18):1240–1261.
20. Kang L, Yu H, Yang X, Zhu Y, Bai X, Wang R, Cao Y, Xu H, Luo H, Lu L *et al*: **Neutrophil extracellular traps released by neutrophils impair revascularization and vascular remodeling after stroke**. Nat Commun 2020, **11**(1):2488.
21. Zhai Y, Ye SY, Wang QS, Xiong RP, Fu SY, Du H, Xu YW, Peng Y, Huang ZZ, Yang N *et al*: **Overexpressed ski efficiently promotes neurorestoration, increases neuronal regeneration, and reduces astrogliosis after traumatic brain injury**. Gene Ther 2022.

22. Miller-Ocuin JL, Liang X, Boone BA, Doerfler WR, Singhi AD, Tang D, Kang R, Lotze MT, Zeh HJ, 3rd: **DNA released from neutrophil extracellular traps (NETs) activates pancreatic stellate cells and enhances pancreatic tumor growth**. Oncoimmunology 2019, **8**(9):e1605822.
23. Wang R, Zhu Y, Liu Z, Chang L, Bai X, Kang L, Cao Y, Yang X, Yu H, Shi MJ *et al*: **Neutrophil extracellular traps promote tPA-induced brain hemorrhage via cGAS in mice with stroke**. Blood 2021, **138**(1):91–103.
24. Sun S, Duan Z, Wang X, Chu C, Yang C, Chen F, Wang D, Wang C, Li Q, Ding W: **Neutrophil extracellular traps impair intestinal barrier functions in sepsis by regulating TLR9-mediated endoplasmic reticulum stress pathway**. Cell Death Dis 2021, **12**(6):606.
25. Chen X, Chen C, Fan S, Wu S, Yang F, Fang Z, Fu H, Li Y: **Omega-3 polyunsaturated fatty acid attenuates the inflammatory response by modulating microglia polarization through SIRT1-mediated deacetylation of the HMGB1/NF-kappaB pathway following experimental traumatic brain injury**. J Neuroinflammation 2018, **15**(1):116.
26. Hu J, Wang X, Chen X, Fang Y, Chen K, Peng W, Wang Z, Guo K, Tan X, Liang F *et al*: **Hydroxychloroquine attenuates neuroinflammation following traumatic brain injury by regulating the TLR4/NF-kappaB signaling pathway**. J Neuroinflammation 2022, **19**(1):71.
27. Wei P, Wang K, Luo C, Huang Y, Misilimu D, Wen H, Jin P, Li C, Gong Y, Gao Y: **Cordycepin confers long-term neuroprotection via inhibiting neutrophil infiltration and neuroinflammation after traumatic brain injury**. J Neuroinflammation 2021, **18**(1):137.
28. Ding R, Li H, Liu Y, Ou W, Zhang X, Chai H, Huang X, Yang W, Wang Q: **Activating cGAS-STING axis contributes to neuroinflammation in CVST mouse model and induces inflammasome activation and microglia pyroptosis**. J Neuroinflammation 2022, **19**(1):137.
29. Zhang LM, Xin Y, Wu ZY, Song RX, Miao HT, Zheng WC, Li Y, Zhang DX, Zhao XC: **STING mediates neuroinflammatory response by activating NLRP3-related pyroptosis in severe traumatic brain injury**. J Neurochem 2022, **162**(5):444–462.
30. McKenzie BA, Mamik MK, Saito LB, Boghozian R, Monaco MC, Major EO, Lu JQ, Branton WG, Power C: **Caspase-1 inhibition prevents glial inflammasome activation and pyroptosis in models of multiple sclerosis**. Proc Natl Acad Sci U S A 2018, **115**(26):E6065-E6074.
31. Jorch SK, Kubes P: **An emerging role for neutrophil extracellular traps in noninfectious disease**. Nat Med 2017, **23**(3):279–287.
32. Gao D, Wu J, Wu YT, Du F, Aroh C, Yan N, Sun L, Chen ZJ: **Cyclic GMP-AMP synthase is an innate immune sensor of HIV and other retroviruses**. Science 2013, **341**(6148):903–906.
33. Martinod K, Demers M, Fuchs TA, Wong SL, Brill A, Gallant M, Hu J, Wang Y, Wagner DD: **Neutrophil histone modification by peptidylarginine deiminase 4 is critical for deep vein thrombosis in mice**. Proc Natl Acad Sci U S A 2013, **110**(21):8674–8679.
34. Jassam YN, Izzy S, Whalen M, McGavern DB, El Khoury J: **Neuroimmunology of Traumatic Brain Injury: Time for a Paradigm Shift**. Neuron 2017, **95**(6):1246–1265.

35. Karve IP, Taylor JM, Crack PJ: **The contribution of astrocytes and microglia to traumatic brain injury**. Br J Pharmacol 2016, **173**(4):692–702.
36. Gyoneva S, Ransohoff RM: **Inflammatory reaction after traumatic brain injury: therapeutic potential of targeting cell-cell communication by chemokines**. Trends Pharmacol Sci 2015, **36**(7):471–480.
37. Rhind SG, Crnko NT, Baker AJ, Morrison LJ, Shek PN, Scarpelini S, Rizoli SB: **Prehospital resuscitation with hypertonic saline-dextran modulates inflammatory, coagulation and endothelial activation marker profiles in severe traumatic brain injured patients**. J Neuroinflammation 2010, **7**:5.
38. Szmydynger-Chodobska J, Strazielle N, Zink BJ, Ghersi-Egea JF, Chodobski A: **The role of the choroid plexus in neutrophil invasion after traumatic brain injury**. J Cereb Blood Flow Metab 2009, **29**(9):1503–1516.
39. Roth TL, Nayak D, Atanasijevic T, Koretsky AP, Latour LL, McGavern DB: **Transcranial amelioration of inflammation and cell death after brain injury**. Nature 2014, **505**(7482):223–228.
40. Baldwin KJ, Hogg JP: **Progressive multifocal leukoencephalopathy in patients with multiple sclerosis**. Curr Opin Neurol 2013, **26**(3):318–323.
41. Hanhai Z, Bin Q, Shengjun Z, Jingbo L, Yinghan G, Lingxin C, Shenglong C, Hang Z, Huaijun C, Jianfeng Z *et al*: **Neutrophil extracellular traps, released from neutrophil, promote microglia inflammation and contribute to poor outcome in subarachnoid hemorrhage**. Aging (Albany NY) 2021, **13**(9):13108–13123.
42. Li P, Li M, Lindberg MR, Kennett MJ, Xiong N, Wang Y: **PAD4 is essential for antibacterial innate immunity mediated by neutrophil extracellular traps**. J Exp Med 2010, **207**(9):1853–1862.
43. Abdullah A, Zhang M, Frugier T, Bedoui S, Taylor JM, Crack PJ: **STING-mediated type-I interferons contribute to the neuroinflammatory process and detrimental effects following traumatic brain injury**. J Neuroinflammation 2018, **15**(1):323.
44. Barrett JP, Knoblach SM, Bhattacharya S, Gordish-Dressman H, Stoica BA, Loane DJ: **Traumatic Brain Injury Induces cGAS Activation and Type I Interferon Signaling in Aged Mice**. Front Immunol 2021, **12**:710608.

Figures

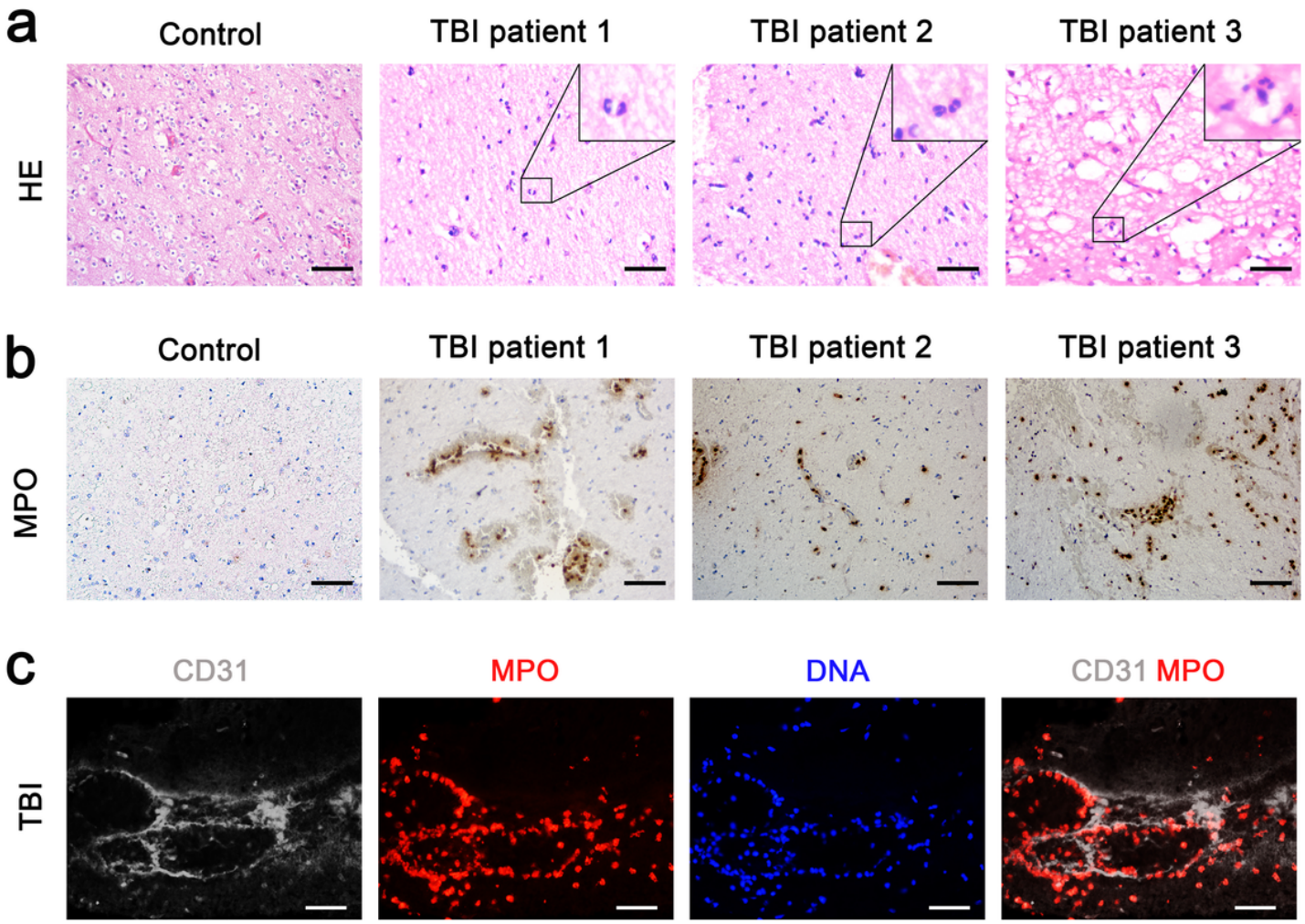

Figure 1

Neutrophils are found in contused brain tissue from TBI patients. **a** Hematoxylin and eosin staining of the peri-injured brain tissue sections from TBI (n=6) and glioma (n=4) patients. Scale bar = 100 μm. **b** Representative immunostaining of MPO-positive neutrophils in the contused brain tissue sections from TBI (n=6) and glioma (n=4) patients. Scale bar = 100 μm. **c** Representative immunofluorescence staining of MPO-positive neutrophils (red) and CD31-labeled blood vessels (white) in the brain tissue sections from TBI patients (n=6). Nuclei were stained with DAPI (blue). Scale bar = 100 μm.

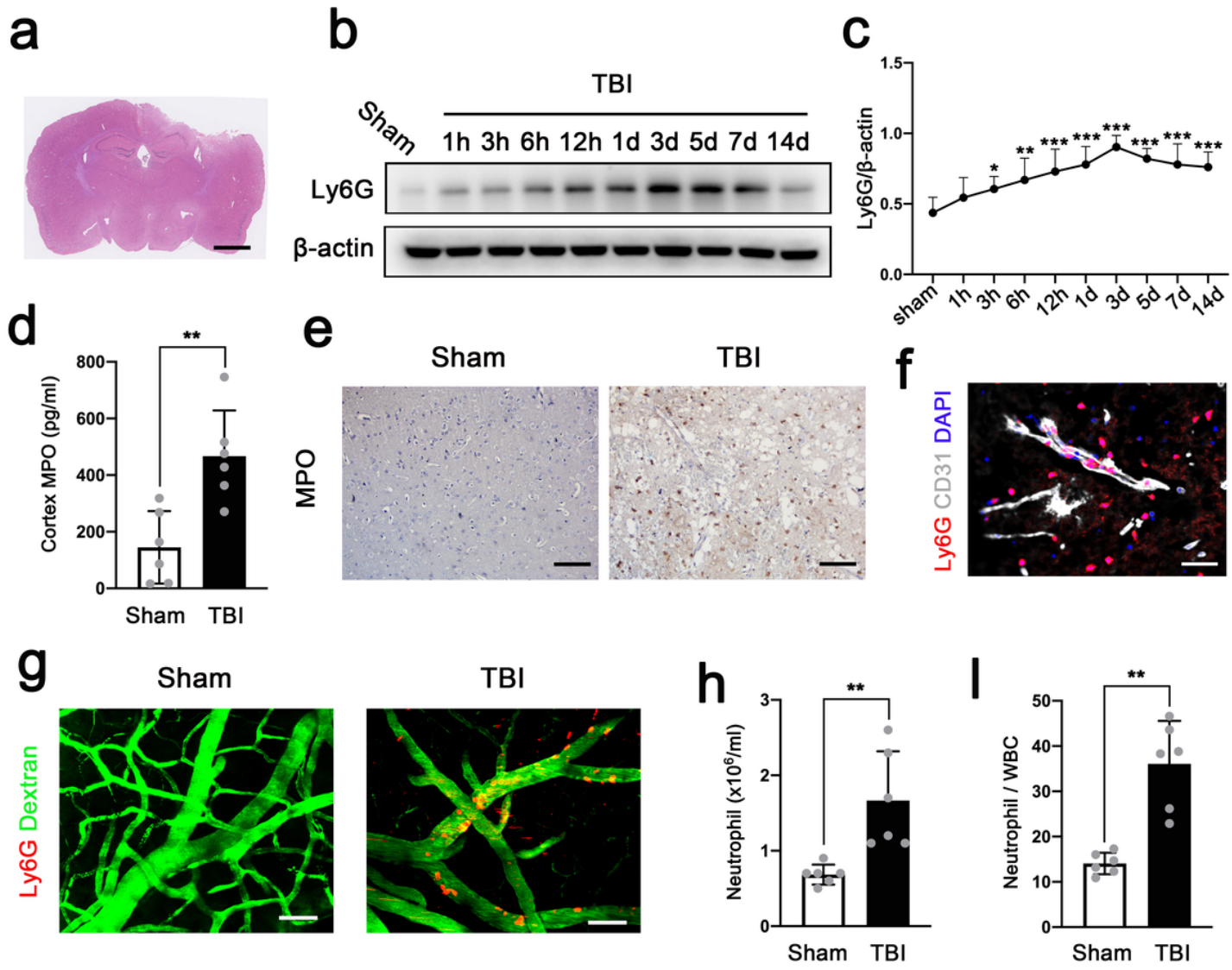

Figure 2

<u>Neutrophils infiltrate in the contused brain parenchyma during all stages of TBI.</u> **a** Hematoxylin and eosin-stained coronal section in the cerebral cortex 3 d after controlled cortical impact (CCI). This photomicrograph shows the severe injury. Scale bar = 2mm. **b, c** Representative immunoblots of the time course of neutrophils appearance **(b)** andquantification of the amount of neutrophil**(c)** in the contused cortex of mice subjected to TBI (n=6).One-way ANOVA test was applied with *P < 0.05, **P < 0.01 and ***P < 0.001 vs. Sham **d** Quantification of MPO protein levelsin the ipsilateral cerebral cortex of mice 3 d after TBI or sham operation (n=6), unpaired two-tailed Student's t-test was applied with **P = 0.0043. **e** Representative immunostaining of MPO-positive neutrophils in the contused cortex of mice at 3 d after TBI, compared with sham-operated mice. Scale bar = 100 μm. Independent experiments are repeated at least three times. **f** Representative immunofluorescence staining of MPO-positive neutrophils (red) and CD31-labeled blood vessels (white) in the contused cortex of mice at 3 d after TBI. Nuclei were stained with DAPI (blue). Neutrophils were observed to infiltrate into the parenchyma. Scale bar = 25 μm. Independent experiments are repeated at least three times. **g** Representative in-vivo multiphoton

microscopy images of neutrophils (red) and cerebral blood vessels (green) around contused cortex of mice 3 d after TBI or sham operation. Neutrophils adhered to the blood vessels and migrated into the parenchyma. Blood vessels (green) were labeled by intravenous injection of FITC-dextran (MW = 2000,000 Da) and neutrophils were labeled by intravenous injection of PE-conjugated monoclonal Ly6G antibody. Scale bar = 100 μm. **h, i** Neutrophil counts **(h)** and percentage of peripheral blood neutrophils **(i)** at 3 d in TBI mice or sham mice were analyzed using a SYSME X Hematology Analyzer. unpaired two-tailed Student's t-test was applied with **P < 0.01 (Sham vs. TBI). Data are represented as mean ± SD.

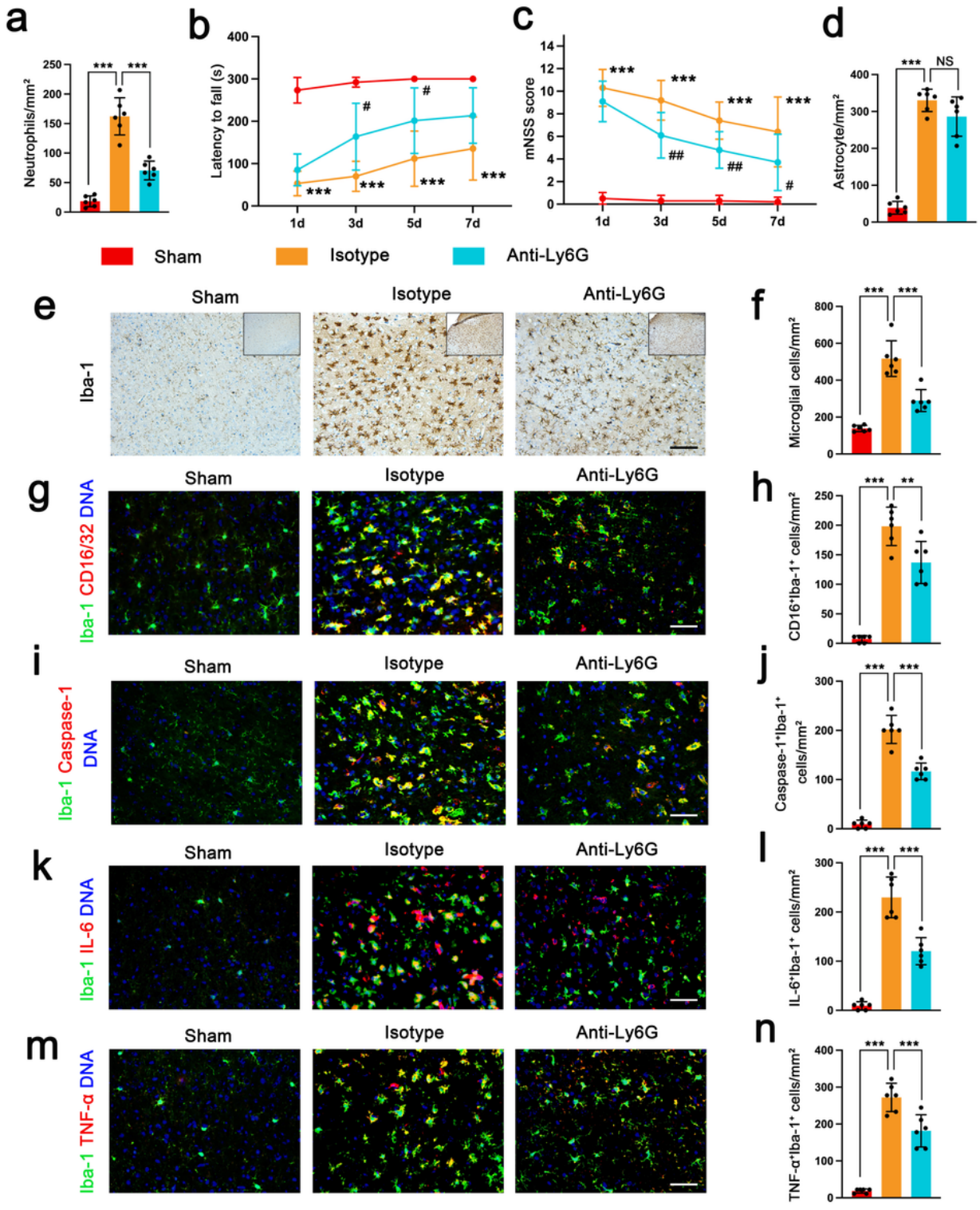

Figure 3

Neutrophil depletion ameliorates activation and M1 polarization of microglia/macrophages after TBI. **a** Quantification of the number of neutrophils in the contused cortex at 3 d in mice treated with isotype or anti-Ly6G antibody compared with the sham operation (n=6). **b, c** Neurological function of mice treated with isotype or anti-Ly6G antibody compared with the sham operation were assessed using the Rotarod test (b) and modified neurological severity scores (c) at 1 d, 3 d, 5 d, 7 d after TBI (n = 10). **d** Quantification of the number of GFAP-positive astrocytes in the contused cortex at 3 d in mice treated with isotype or anti-Ly6G antibody compared with the sham operation (n=6). **e, f** Representative immunostaining of Iba-1-positive microglia/macrophages **(e)** and quantification of the amounts of Iba-1-positive microglia/macrophages **(f)** in the contused cortex of mice (n=6). Scale bar = 100 μm**. g, h** Representative immunofluorescence images **(g)** of Iba-1-positive microglia/macrophages (green) and CD16/32-positive cells (red) and quantitative analysis **(h)** of CD16/32-positive microglia/macrophages in the contused cortex of mice (n=6). Nuclei were stained with DAPI (blue). Scale bar = 50 μm**. i, j** Representative immunofluorescence images **(i)** of Iba-1-positive microglia/macrophages (green) and caspase-1-positive cells (red) and quantitative analysis **(j)** of caspase-1-positive microglia/macrophages in the contused cortex of mice (n=6). Nuclei were stained with DAPI (blue). Scale bar = 50 μm**. k, l** Representative immunofluorescence images **(k)** of Iba-1-positive microglia/macrophages (green) and IL-6-positive cells (red) and quantitative analysis **(l)** of IL-6-positive microglia/macrophages in the contused cortex of mice (n=6). Nuclei were stained with DAPI (blue). Scale bar = 50 μm**. m, n** Representative immunofluorescence images **(m)** of Iba-1-positive microglia/macrophages (green) and TNF-α-positive cells (red) and quantitative analysis **(n)** of TNF-α-positive microglia/macrophages in the contused cortex of mice (n=6). Nuclei were stained with DAPI (blue). Scale bar = 50 μm**.** Data are represented as mean ± SD. *P < 0.05, **P < 0.01 and ***P < 0.001 compared within two groups. $^{\#}$p < 0.05, $^{\#\#}$p < 0.01 and vs Isotype group.

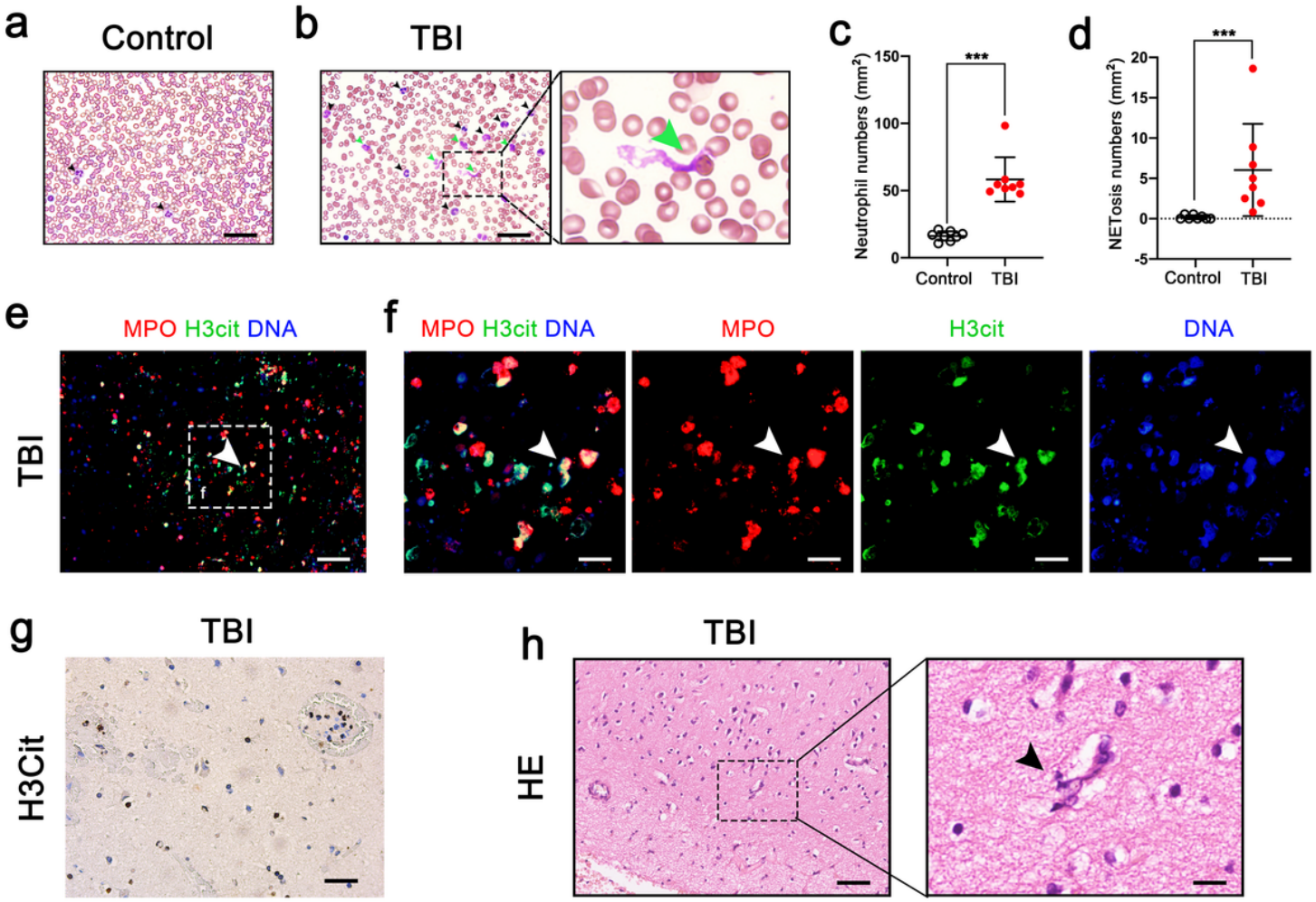

Figure 4

Neutrophil extracellular traps (NETs) are found in circulating blood and contused brains from TBI patients. a-d Representative images Wright-stained peripheral blood smears from healthy donors **(a)** and TBI **(b)** patients, and quantitative analysis of neutrophil counts (c) and NETosis (d) in blood smears. Black arrows indicate neutrophils, green arrows indicate extracellular DNA fibers. Scale bar = 50 μm. Unpaired two-tailed Student's t-test was applied with **P < 0.001(c) (Control vs. TBI), **P < 0.001(d) (Control vs. TBI). e, f Representative immunofluorescence images (e) showing the NET formation (H3Cit-positive neutrophils) in the brain tissue sections from TBI patients. The inset is magnified on the right side (f). Arrows indicate NETs. Neutrophils were labeled with MPO (red), NETs were labeled with H3Cit (green) and Nuclei were stained with DAPI (blue). Independent experiments are repeated at least three times. Bar =100μm **(e)** and 25μm **(f)**. g Representative immunostaining of H3Cit -positive neutrophils in the contused brain tissue sections from TBI patients. Independent experiments are repeated at least three times. Scale bar = 100 μm. h Hematoxylin and eosin staining of the contused brain tissue sections from TBI patients. The inset is magnified on the right side. Arrows indicate extracellular DNA fibers. Scale bar =100μm (left) and 25μm (right).

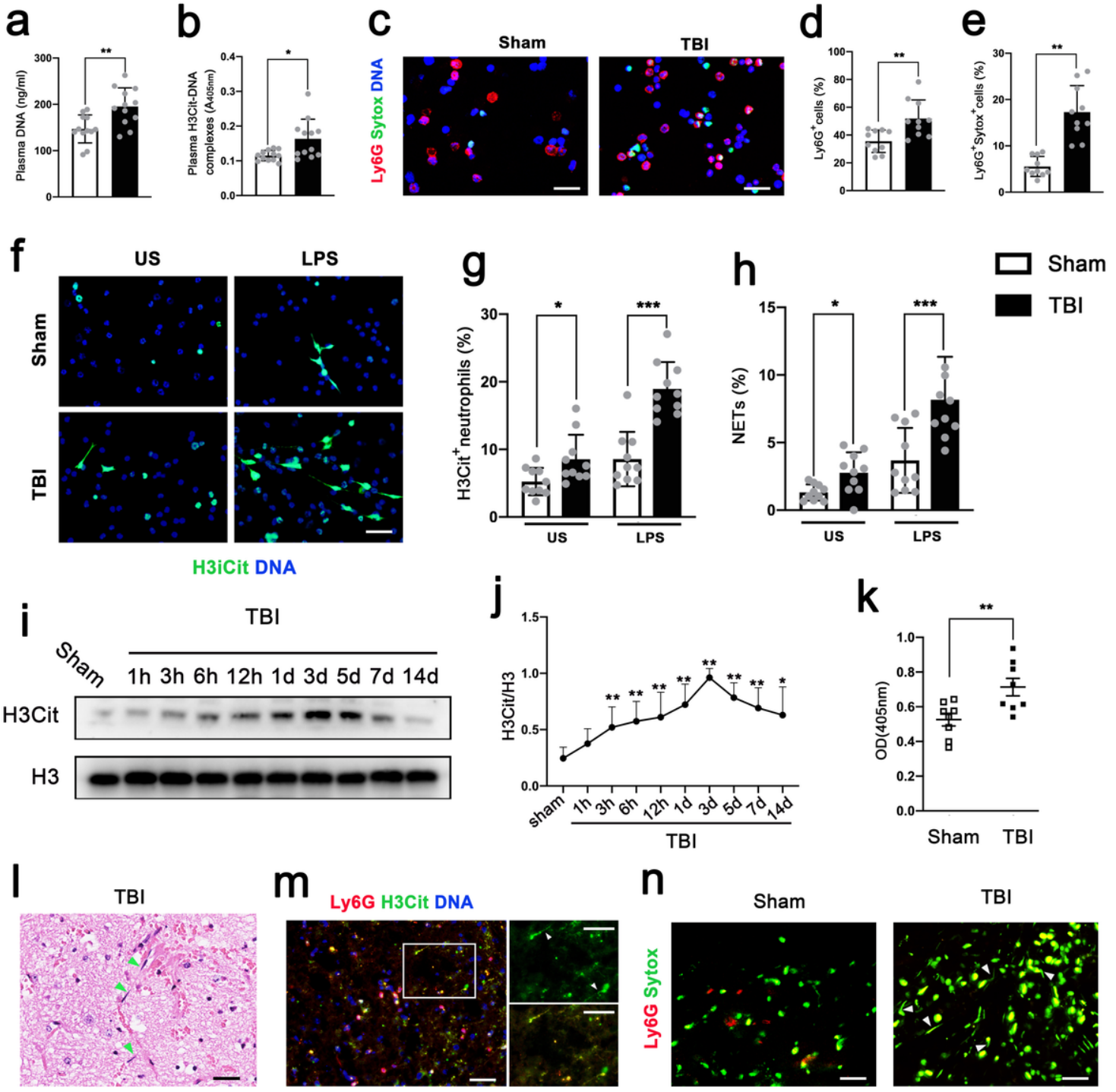

Figure 5

Neutrophil extracellular traps (NETs) are detected in circulating blood and contused cortex in mice with TBI. **a, b** Levels of plasma DNA **(a)** and plasma H3Cit-DNA complex **(b)**were elevated at 3 d after TBI (n = 12). **c** Representative images of Sytox (green) and Ly6G (red) double-positive cells in cytospins from sham-operated mice and TBI mice at 3 d. Bar = 25 μm. **d, e** Quantification of Ly6G-positive neutrophils in the total cell population **(d)** and the percentage of Sytox-positive neutrophils **(e)** in cytospins (n = 10). **f** Neutrophils were incubated in the presence or absence of Klebsiella pneumonia lipopolysaccharide for

2.5 h and stained with H3Cit (green) and DAPI (blue). Arrows indicate NETs. US, unstimulated. Bar = 50 μm. **g, h** Quantification of the percentage of H3Cit-positive neutrophils (g) and NETs (h) in total neutrophils (n = 10). **i,j** Representative immunoblots of the time course of NETs appearance **(i)** and quantification of the H3Cit levels (j) in the contused cortex of mice subjected to TBI, compared with sham-operated mice (n=6). **P < 0.01 (Sham vs. 3h), **P < 0.01 (Sham vs. 6h), **P < 0.01 (Sham vs. 12h), **P< 0.01 (Sham vs. 1d), **P< 0.01 (Sham vs. 3d), **P< 0.01 (Sham vs. 5d), **P< 0.01 (Sham vs. 7d), *P< 0.05 (Sham vs. 14d). **k** Quantification of the H3Cit-DNA complex levels in the contused cortex of mice subjected to TBI, compared with sham-operated mice (n=6). **l** Hematoxylin and eosin sections showing the presence of extracellular DNA (arrows) in the contused cortex at 3 d after TBI. Independent experiments are repeated at least three times. Scale bar = 50 μm. **m** Representative immunofluorescence images of H3Cit (green) and Ly6G (red) double-positive cells in brain sections from TBI mice at 3 d. Nuclei were stained with DAPI (blue). The inset is magnified on the right side. Arrows indicate NETs. Bar = 50 μm (left) and20 μm (right). **n** Representative in-vivo multiphoton microscopy images of extracellular DNA and neutrophils around the contused cortex of TBI mice or sham mice at 3 d. Extracellular DNA (green) was labeled with intravenous injection of Sytox and neutrophils (red) with intravenous injection of PE-conjugated monoclonal Ly6G antibody. Arrows indicate extracellular DNA fibers. Independent experiments are repeated at least three times. Bar = 50 μm. Data are presented as mean ± SD. *P < 0.05, **P < 0.01 and ***P < 0.001 compared within two groups.

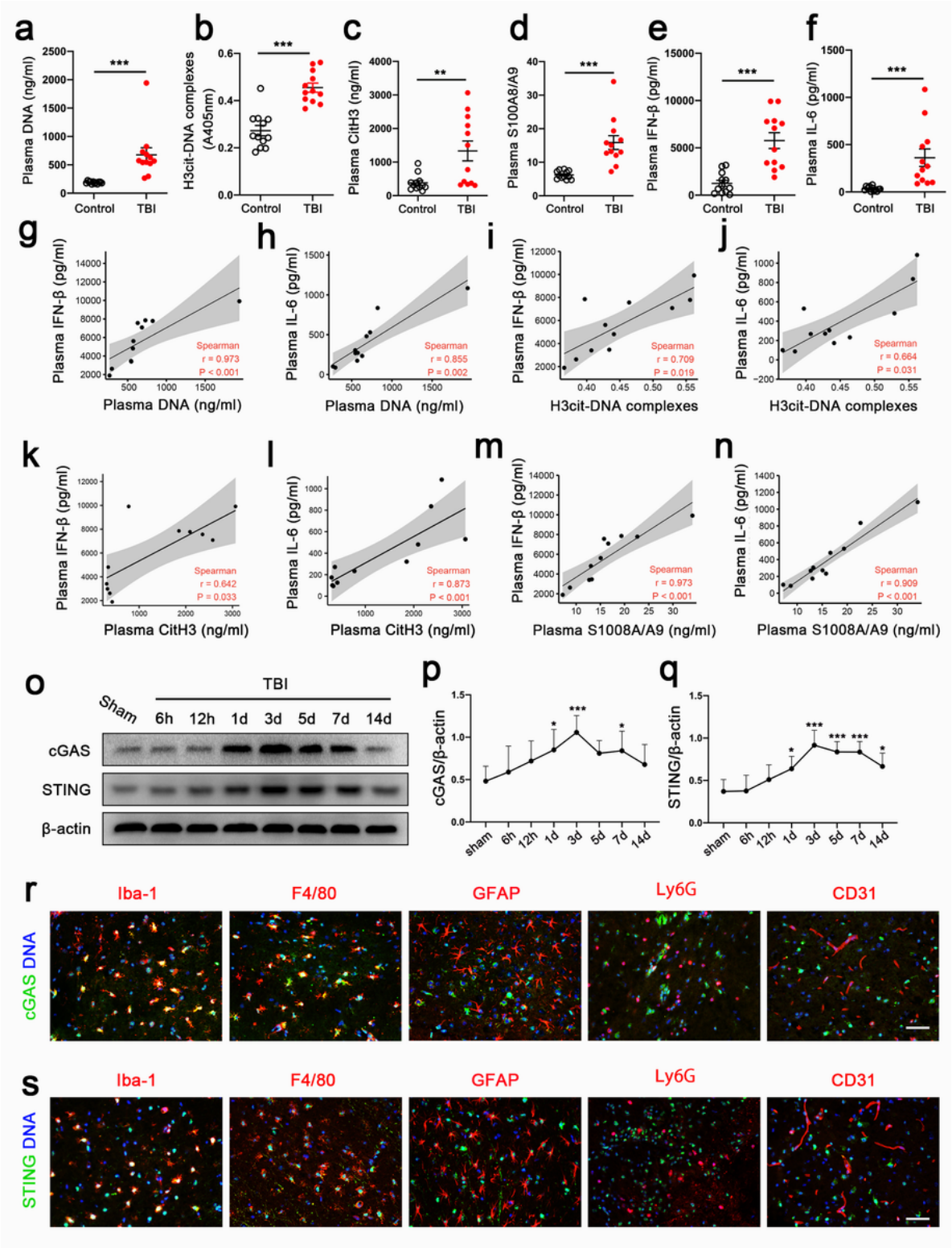

Figure 6

Levels of circulating NET markers correlate with levels of plasma STING-related IFN-β and IL-6 in the peripheral blood of patients with TBI. a-f Quantification of the Levels of plasma DNA (a), plasma H3Cit-DNA complex (b),plasma H3Cit (c), plasma S1008A/A9(d), plasma IFN-β(e), plasma IL-6(f) in the peripheral blood of healthy donors (n = 12) and TBI patients (n = 12). **g-n** Correlation among the levels of plasma DNA, plasma H3Cit-DNA complex, plasma H3Cit, and plasma S1008A/A9 with levels of plasma

IFN-βand plasma IL-6. Spearman correlation analysis was applied with r=0.973, P < 0.001 (g) (plasma DNA correlate with plasma IFN-β), r=0.855, P=0.002 (h) (plasma DNA correlate with plasma IL-6), r=0.709, P=0.019 (i) (plasma H3Cit-DNA complex correlate with plasma IFN-β), r=0.664, P=0.031 (j) (plasma H3Cit-DNA complex correlate with plasma IL-6), r=0.642, P=0.033 (k) (plasma H3Cit correlate with plasma IFN-β), r=0.873, P < 0.001 (l) (plasma H3Cit correlate with plasma IL-6), r=0.973, P < 0.001 (m) plasma S1008A/A9 correlate with plasma IFN-β), r=0.909, P < 0.001 (n) (plasma S1008A/A9 correlate with plasma IL-6). **o-q** Representative immunoblots of the time course of cGAS and STING appearance **(o)** and densitometric analysis of the relative expressions of the cGAS (p) and STING (q) in the contused cortex of mice subjected to TBI, compared with sham-operated mice (n=6). One-way ANOVA test was applied with **P < 0.001 (q) (Sham vs. 3d), *P < 0.05 (q) (Sham vs. 7dh), *P < 0.05 (q) (Sham vs. 1d), ***P< 0.001 (q) (Sham vs. 3d), **P< 0.001 (q) (Sham vs. 5d), **P< 0.001 (q) (Sham vs. 7d), *P < 0.05 (q) (Sham vs. 14d). **r,s** Representative double immunostaining images of cGAS (green) and STING (green) with microglial cells (Iba1, red), macrophages (F4/80, red), astrocytes (GFAP, red), neutrophils (Ly6G, red) and endotheliocytes (CD31, red) in mice subjected to TBI. Nuclei were stained with DAPI (blue). Independent experiments are repeated at least three times. Scale bar, 50mm. Data are presented as mean ± SD.

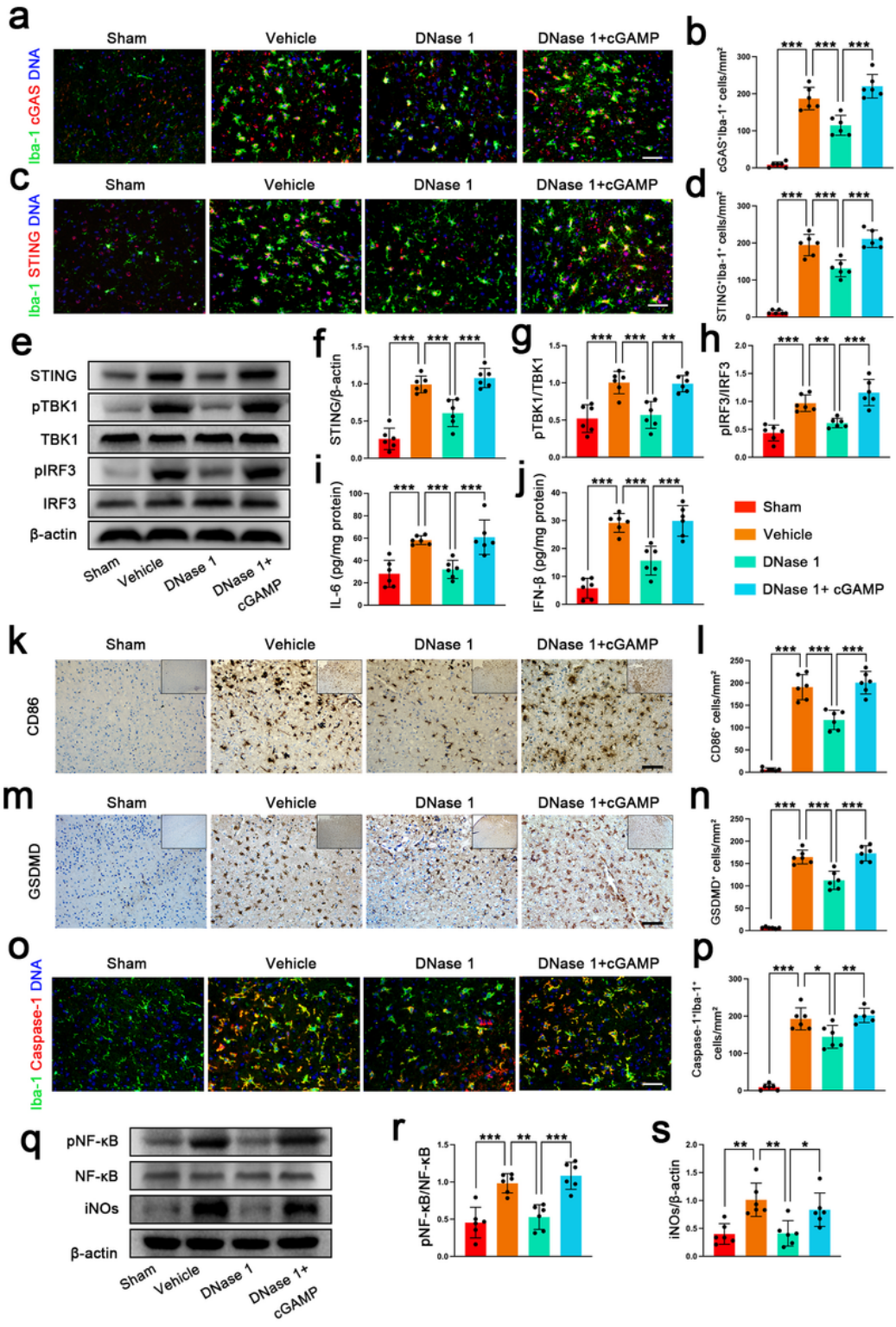

Figure 7

DNase 1 ameliorates activation and M1 polarization of microglia/macrophages by inhibiting the cGAS-STING pathway a, b Representative immunofluorescence images **(a)** of Iba-1-positive microglia/macrophages (green) and cGAS -positive cells (red) and quantitative analysis **(b)** of cGAS-positive microglia/macrophages in the contused cortex of mice at 3 d (n=6). Nuclei were stained with DAPI (blue). Scale bar = 50 μm**. c, d** Representative immunofluorescence images **(a)** of Iba-1-positive

microglia/macrophages (green) and STING-positive cells (green) and quantitative analysis **(b)** of STING-positive microglia/macrophages in the contused cortex of mice at 3 d (n=6). Scale bar = 50 μm. **e-h** Representative immunoblot bands of STING, pTBK1, and pIRF3 and densitometric analysis of the relative expressions of STING**(f),** pTBK1**(g)**, and pIRF3 **(h)** in the contused cortex of mice at 3 d (n=6). **i,j** Quantitative analysis of IFN-β(i) and IL-6 (j) in the contused cortex of mice at 3 d (n=6). **k,l** Representative immunostaining (k) of CD86 -positive cells and quantitative analysis (l) of CD86 -positive cells in the contused cortex of mice at 3 d (n=6). Scale bar = 100 μm. **m,n** Representative immunostaining (m) of GSDMD-positive cells and quantitative analysis (n) of GSDMD-positive cells in the contused cortex of mice at 3 d (n=6). Scale bar = 100 μm. **o, p** Representative immunofluorescence images **(o)** of Iba-1-positive microglia/macrophages (green) and caspase-1 -positive cells (red) and quantitative analysis **(p)** of caspase-1 -positive microglia/macrophages in the contused cortex of mice at 3 d (n=6). Scale bar = 50 μm**. q-s** Representative immunoblot bands (q) of pNF-κB and iNOs and densitometric analysis of the relative expressions of pNF-κB (r) and iNOs **(s)** in the contused cortex of mice at 3 d (n=6). Data are presented as mean ± SD. *P < 0.05, **P < 0.01 and ***P < 0.001 compared within two groups.

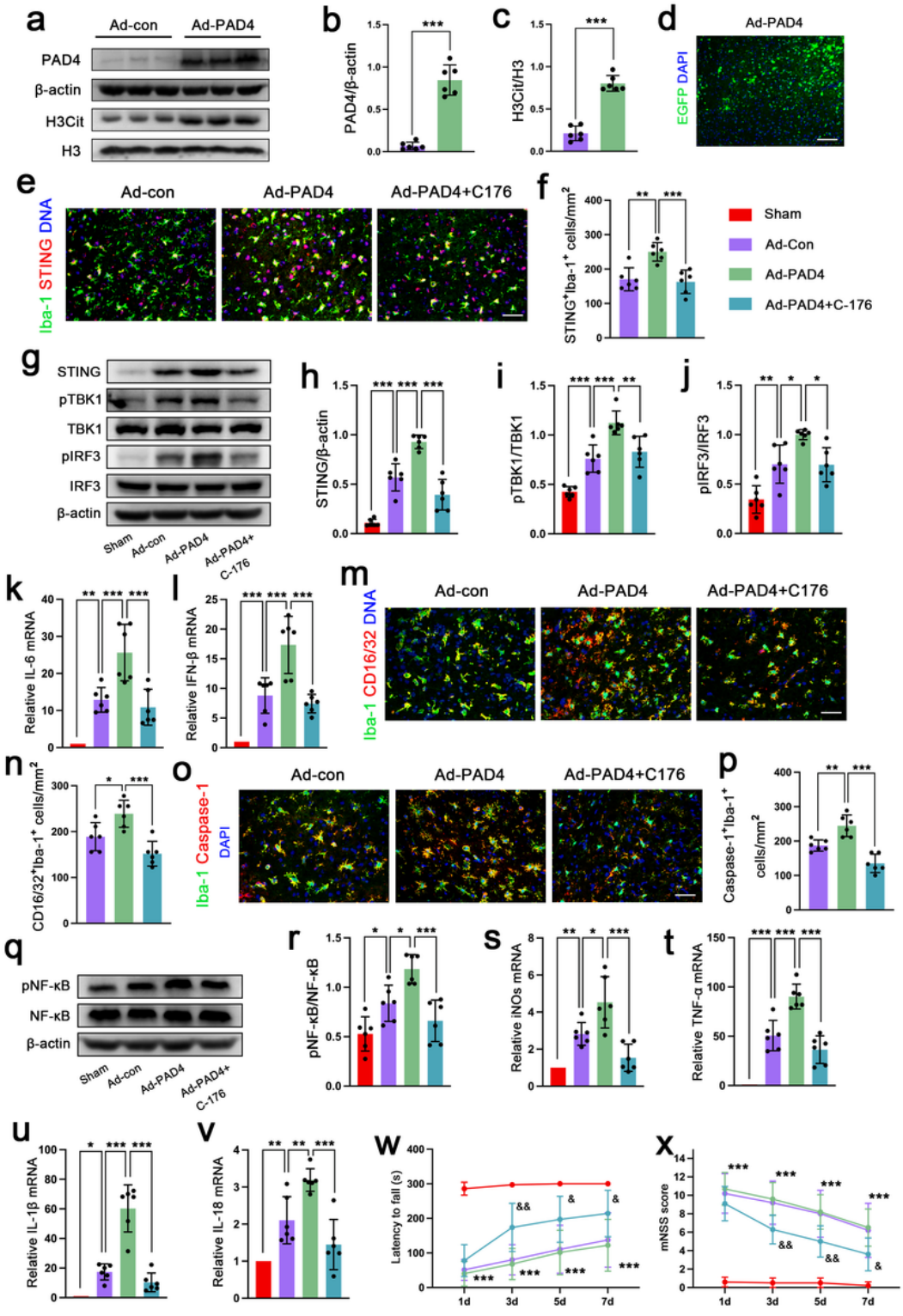

Figure 8

<u>Overexpression of PAD4 exacerbates activation and M1 polarization of microglia/macrophages by promoting the cGAS-STING pathway activation.</u> **a-c** Representative immunoblot bands of PAD4, and H3Cit and densitometric analysis of the relative expressions of PAD4 (b), and H3Cit (c) in the contused cortex of mice at 3 d after injection of control (Ad-Con) or PAD4 adenovirus (Ad-PAD4) (n=6). d Representative images of recombinant Adeno-PAD4-EGFP-infected cells in the contused cortex 3 d after

injection. Nuclei were stained with DAPI (blue). Scale bar = 100 μm. e, f Representative immunofluorescence images (e) of Iba-1-positive microglia/macrophages (green) and STING-positive cells (green) and quantitative analysis **(f)** of STING-positive microglia/macrophages in the contused cortex of mice at 3 d (n=6). Nuclei were stained with DAPI (blue). Scale bar = 50 μm. **g-j** Representative immunoblot bands (g) of STING, pTBK1, and pIRF3 and densitometric analysis of the relative expressions of STING**(h),** pTBK1**(i)**, and pIRF3 **(j)** in the contused cortex of mice at 3 d (n=6). **k,l** Quantitative analysis of mRNA level of IL-6 (k) and IFN-β(l) in the contused cortex of mice at 3 d (n=6). **m, n** Representative immunofluorescence images **(m)** of Iba-1-positive microglia/macrophages (green) and CD16/32 -positive cells (red) and quantitative analysis **(n)** of CD16/32 -positive microglia/macrophages in the contused cortex of mice at 3 d (n=6). Scale bar = 50 μm**. o, p** Representative immunofluorescence images **(o)** of Iba-1-positive microglia/macrophages (green) and caspase-1-positive cells (red) and quantitative analysis **(p)** of caspase-1 -positive microglia/macrophages in the contused cortex of mice at 3 d (n=6). Nuclei were stained with DAPI (blue). Scale bar = 50 μm**. q, r** Representative immunoblot bands (q) of pNF-κB and densitometric analysis (r) of the relative expressions of pNF-κB in the contused cortex of mice at 3 d (n=6). **r-v** Quantitative analysis of mRNA level of iNOs (s), TNF-α (t), IL-1β (u) and IL-18 (v) in the contused cortex of mice at 3 d (n=6). **w, x** Neurological function was assessed using the Rotarod test (w) and modified neurological severity scores (x) at 1 d, 3 d, 5 d, 7 d after TBI (n = 10). Data are presented as mean ± SD. *P < 0.05, **P < 0.01 and ***P < 0.001 compared within two groups. $^{\&}$p < 0.05, $^{\&\&}$p < 0.01 and vs Ad-PAD4 group.

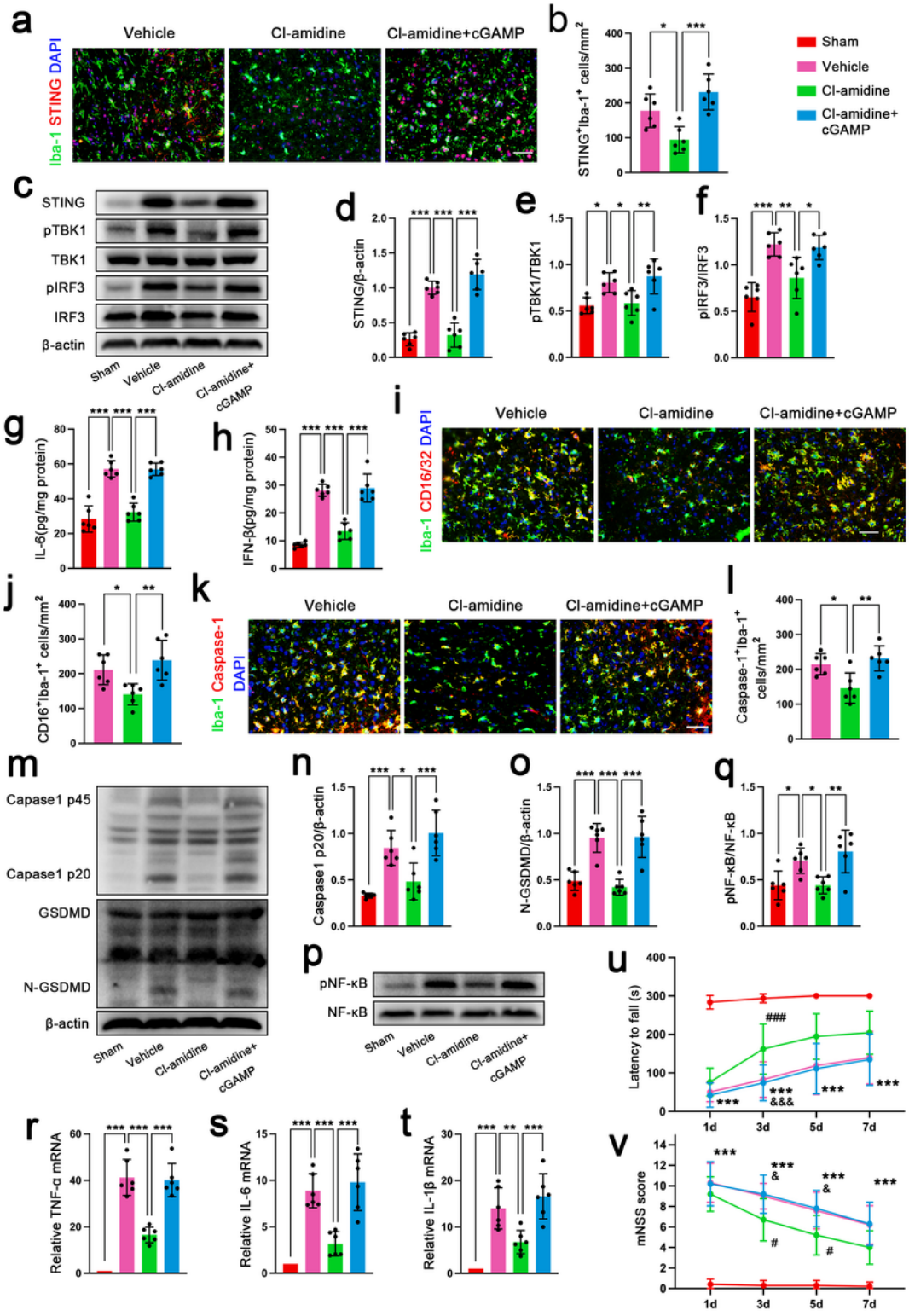

Figure 9

Inhibition of PAD4 ameliorates activation and M1 polarization of microglia/macrophages after TBI.

a, b Representative immunofluorescence images **(a)** of Iba-1-positive microglia/macrophages (green) and STING-positive cells (green) and quantitative analysis **(b)** of STING-positive microglia/macrophages in the contused cortex of mice at 3 d (n=6). Nuclei were stained with DAPI (blue). Scale bar = 50 μm. **c-f**

Representative immunoblot bands of STING, pTBK1, and pIRF3 (c) and densitometric analysis of the relative expressions of STING**(d),** pTBK1**(e)**, and pIRF3 **(f)** in the contused cortex of mice at 3 d (n=6). **g,h** Quantitative analysis of IFN-β(g) and IL-6 (h) in the contused cortex of mice at 3 d (n=6). **i,j** Representative immunofluorescence images **(i)** of Iba-1-positive microglia/macrophages (green) and CD16/32 -positive cells (red) and quantitative analysis **(j)** of CD16/32 -positive microglia/macrophages in the contused cortex of mice at 3 d (n=6). Nuclei were stained with DAPI (blue). Scale bar = 50 μm**. k, l** Representative immunofluorescence images **(k)** of Iba-1-positive microglia/macrophages (green) and caspase-1-positive cells (red) and quantitative analysis **(l)** of caspase-1 -positive microglia/macrophages in the contused cortex of mice at 3 d (n=6). **m-o** Representative immunoblot bands (m) of caspase1 p20 and N-GSDMD and densitometric analysis of the relative expressions of caspase1 p20 **(n) and** N-GSDMD **(o)** in the contused cortex of mice at 3 d (n=6). **p,q** Representative immunoblot bands (p) of pNF-κB and densitometric analysis (q) of the relative expressions of pNF-κB in the contused cortex of mice at 3 d (n=6). **r-t** Quantitative analysis of mRNA level of TNF-α (r), IL-6 (s), and IL-1β (t) in the contused cortex of mice at 3 d (n=6). **u,v** Neurological function was assessed using the Rotarod test (u) and modified neurological severity scores (v) at 1 d, 3 d, 5 d, 7 d after TBI (n = 10). Data are presented as mean ± SD. *P < 0.05, **P < 0.01 and ***P < 0.001 compared within two groups. $^{\#}$p < 0.05, $^{\#\#\#}$p < 0.001 and vs Isotype group. $^{\&}$p < 0.05, $^{\&\&\&}$p < 0.001 and vs Ad-PAD4 group.

Supplementary Files

This is a list of supplementary files associated with this preprint. Click to download.

- Supplementaryfile1.docx
- uncroppedgelandblotimages1.pdf
- uncroppedgelandblotimages2.pdf
- uncroppedgelandblotimages3.pdf
- uncroppedgelandblotimages4.pdf
- uncroppedgelandblotimages5.pdf
- uncroppedgelandblotimages6.pdf